مجلة العلوم الشاملة

Journal of Total Science

Higher Institute of Science & Technology

Raqdalen, Libya

البحوث المنشورة باللغات الأجنبية

Research Papers in Foreign Languages

Volume (6), supplement Issue (23), (Mar. 2023)

Contents

Research Papers Published in Foreign Languages

Journal of Total Science
Volume (6), Issue (24) (June. 2023)
ISSN: 2518-5799

مجلة العلوم الشاملة
المجلد (6)، العدد (24)، (يونيو2023)
ردمد: 2518-5799

Analysis Short Term Load Forecasting using Fuzzy Logic and Artificial Neural Network

Naji Ammar Eltawil

Higher Institute for Water Technology, Agelat

Abstract— Short term load forecasting is an essential part of the load forecasting and power system planning in recent years has become one of the key areas of research in the field of electrical power system. This paper presents the Short term load of load forecasting using fuzzy logic (FL) and artificial neural network (ANN). FL and ANN are used to forecast short term load. ANN is used to improve the results from FL. And Study the effects of temperature, next one – day load and previous load on short term load forecasting. The simulation is done by the Simulink environment of MATLAB software.

Index Terms— Artificial Neural Networks (ANN); Fuzzy Logic (FL); Load Forecasting.

1. INTRODUCTION.

In power system network load forecasting is very important part of energy management system for operation and planning purpose. Load forecasting means that the techniques for predication of electric load. Load forecasting is integral and central process in the planning and operation of

electric energy management system (5). Therefore, it has becomes an important tool for power companies as it gives foresight of consumers' hourly, daily, weekly and even seasonal demand. This in turn helps the company to plan maintenance schedule and operation, thereby guaranteeing energy satisfaction (6).

2. Load Forecasting – Types

Electric load forecasting is of three types based on duration:

- Short – term load forecasting (STLF)
- Medium – term load forecasting (MTLF)
- Long – term load forecasting (LTLF)

The short-term forecasting is mainly meant for sufficient scheduling and operation of power systems. It is of more importance for a proper and profitable management of the electrical utility. The two important necessities of short-term load forecasting are its high accuracy and faster response to study the characteristics of the electrical loads and the various factors affecting them. Those factors may include climatic changes, season and pricing that have a complicated relationship with the loads. The main objective of short –term load forecast (STLF) is economic load dispatch, load scheduling, reliability and system security assessment. STLF has high forecasting accuracy, and speed response are both significant to analyze the load characteristics, this type of prediction is concerned about control on energy transaction, security, fuel consumption, maintenance, unit scheduling and others. Similarly, there are varieties of functions in this regard such as regulation of smooth load flow, overloading, and blackouts. Time factor impacts electric power system at various daily periods,

weekdays and weekends, holidays, and year's seasons. Here, the time-dependent electric power system discrepancy can reflect the people's manner of living, such as their work schedules, free time, sleeping patterns, etc. (1,8, 9,).

3- Methods of load forecasting

A. FUZZY Logic (FL)

The fuzzy logic model maps the highly non-linear relationship between the weather parameters and their impact on the daily electric load peak. Figure 1 shows the proposed block diagram of the fuzzy model has Several departments like: temperature, humidity, previous day load, wind speed and time, these are fed into the fuzziffier, then the output of the fuzziffier and the fuzzy rule formulated are also fed into the fuzzy inference system (FIS) where all the information are processed. The output of the FIS is fed to the defuzzification where the crisp value of the forecasted load is produced (6).

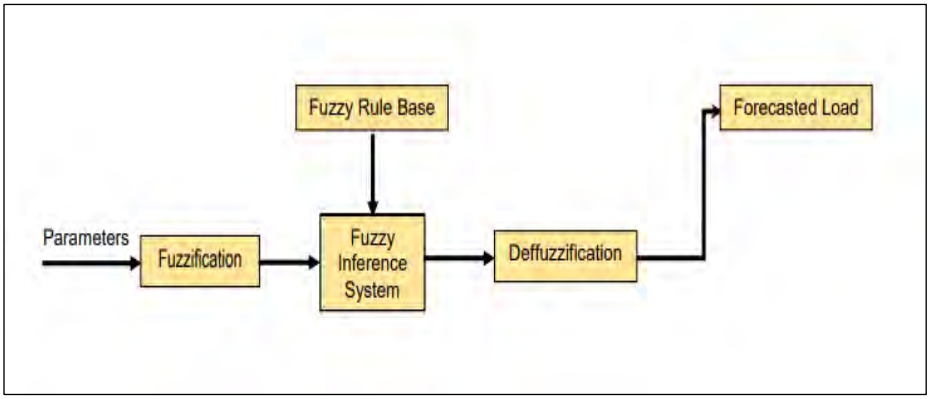

Figure 1: Block Diagram Fuzzy Logic for Short Term Load Forecasting

B. Artificial Neural Networks (ANN)

This is a unique modeling tool that handles complex data inputs and outputs, and historically this was designed to act like the human 'intelligence.' The similarities between the ANN and the human brain: Knowledge comes from learning; and that the knowledge is stored in synaptic weights and this is the beginning of the brain related product. The ANN is a remarkable advancement in the computational industry. Neurons as the core element, pick input, process it, and conduct all the operations and extract the final output. The main components of the inputs are the temperature, humidity, time, , the previous day load, next one day load ,hour of the day. The ANN is being issued for load forecasting yet a significant amount of error is made due to distortion in the fluctuations in load and temperatures. The neural networks are easily compatible with sensory data dealing. The neural networks is a mathematical model with it operates and looks similarly like the brain. It contains unit 'cells' or 'nodes' which netted together. When the inputs (cells) are triggered, the signals go through the network through a note-to-note and exit the network through another particular node. These computational nodes are not linear. The neural network models were grouped into network topology, attributes of node, training or rules of learning as seen in Figure 2.

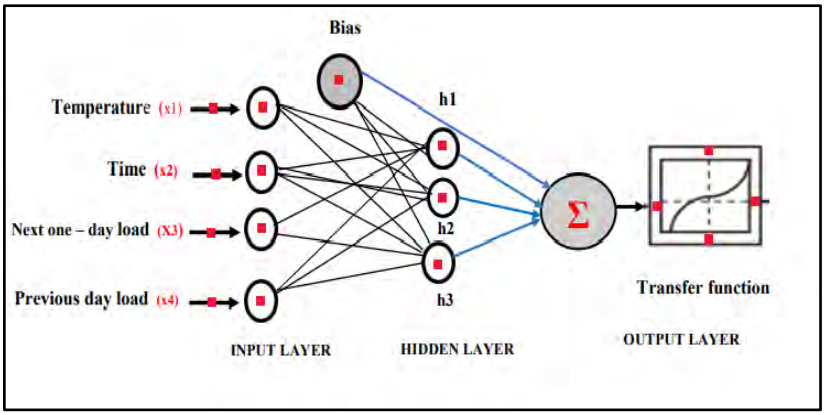

Figure 2: Simulation diagram of Simulink

C. METHODOLOGY

1-Short Term Load Forecasting (24 hours)

The data for every hour was collected for a three-day period (day one, day two, and day three, 2016) from two departments. The electrical load data was gathered from maintenance unit, and the weather parameter (temperature) was obtained from the geography department in Adamawa State, Mubi, Nigeria as shown in Figure 3 (3)

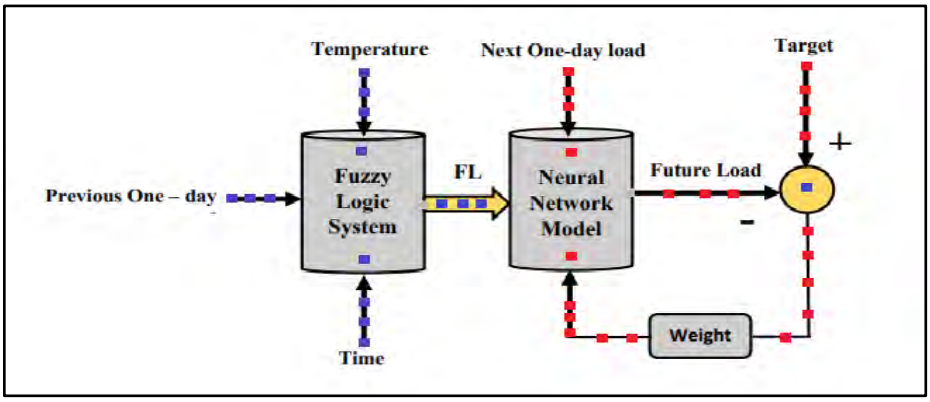

Figure 3: Block diagram representation

Temperature, time and Previous Day – Load are fused into the fuzzy logical system; then an output is obtained then inserted into the neural networks with the Next One – Day Load and target. The output (load predictive) of the network is then compared to the desired production and the weight adjustment through the network to obtain the right or appropriate mapping. Fuzzification this model mirrors the link between weather parameter and how they affect the daily electric power load. The inputs are time, temperature and Previous Day – Load are directly correlated to the electric load peak. Under this review, the hypothesis is that the time has a stronger effect and it is the first input to the fuzzy logic model that carries membership functions of seven (7MF) which are overlapping with a time range. However, with the temperature input, it has three classes of membership functions. Table 1 shows this classification (10). The Tan-sigmoid Transfer Function is used in this papr due to its flexible value (−1 and 1). In this papr, the triangular membership function is adopted, this membership function is flexible on all kinds of data. This is the reason for its considerate. The input data are classified as shown in Table 2. Table 1 Time classification (Hours) Classification Time(Hours) Midnight 0.00 – 3.00 Dawn 4.00 – 6.00 Morning 7.00 – 11.00 Noon 12.00 – 14.00 Evening 15.00 – 17.00 Dusk 18.00 – 20.00 Night 21.00 – 23.00 Table 2 Classifications of Temperature (^{o} C) and Previous Day Load (kW) Classifications Low Medium High Load (kW) (60 – 95) , (90 – 11) , (110 – 125) Temperature (ºC) (20 – 24) , (23 – 27) , (26 – 30) Membership function has several types that are used in fuzzy logical (FLC) like Gaussian, trapezoidal, triangular as shown in Figure 4 (10). The use triangular for this work and the value of mapping is usually between (0, 1).

Table 1: Time classification (Hours)

Classification	Midnight	Dawn	Morning	Noon	Evening	Dusk	Night
Time (Hours)	0.00 – 3.00am	4.00– 6.00am	7.00– 11.00am	12.00– 14.00pm	15.00– 17.00pm	18.00– 20.00pm	21.00– 23.00pm

Table 2: Classifications of Temperature (^0C) and Previous Day Load (kW)

N0	Classifications	Temperature (^0C)	Load (kW)
1	Low	20–24	60–95
2	Medium	23–27	90–115
3	High	26–30	110–125

Membership function has several types that are used in fuzzy logical (FLC) like Gaussian, trapezoidal, triangular as shown in Figure 4 [10]. The use triangular for this papr and the value of mapping is usually between (0,1)

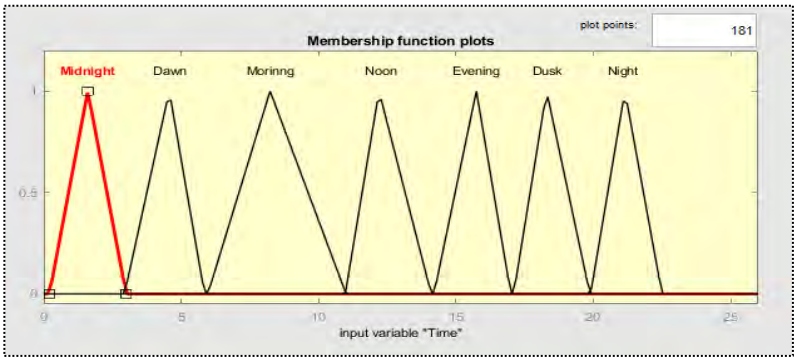

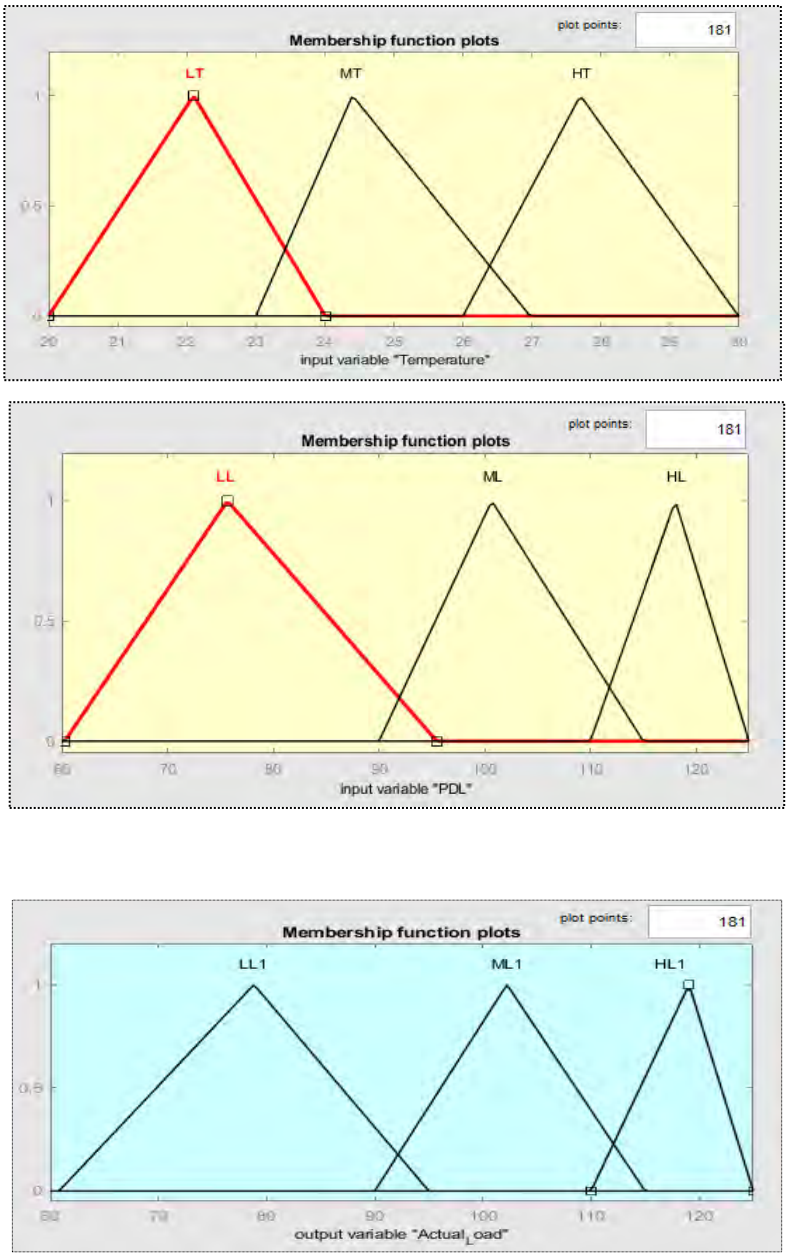

Figure 4: Membership Function Plots For Time, Temperature and Previous Day – Load

Formation of fuzzy rule base: This is the heart of the fuzzy inference system, the heuristic knowledge of the forecast is stored regarding "IF – THEN" rules, it sends information to the fuzzy inference system, which evaluates the received information and computes the forecasted output, in this case, load in kW. The rules base is composed based on the variation of the input parameters. The fuzzy rule base is developed as follows.

1. IF (time is Midnight) and (Temperature is LT) and (PDL is LL) Then (Actual Load) is LL1.
2. •IF (time is Midnight) and (Temperature is LT) and (PDL is ML) Then (Actual Load is ML1.
3. IF (time is Morning) and (Temperature is MT) and (PDL is LL) Then (Actual Load is ML1.
4. IF (time is Morning) and (Temperature is MT) and (PDL is HL) Then (Actual Load is HL1.
5. IF (time is Noon) and (Temperature is HT) and (PDL is HL) Then (Actual Load is HL1.
6. IF (time is Evening) and (Temperature is MT) and (PDL is HL) Then (Actual Load is HL1.
7. IF (time is Dusk) and (Temperature is LT) and (PDL is ML) Then (Actual Load is HL1.
8. IF (time is Dusk) and (Temperature is LT) and (PDL is ML1) Then (Actual Load is ML1.
9. IF (time is Night) and (Temperature is LT) T and (PDL is LL) Then (Actual Load is LL1.

List of Symbols and Abbreviations Parameters

LT	Low Temperature
MT	Medium Temperature
HT	High Temperature
LL	Low Load
ML	Medium Load
HL	High Load
PDL	Previous Day – Load
FLC	Fuzzy Logical

2-The building of Fuzzy Logic Simulation Model between Time and Temperature and Previous Day Load (short-term for one day).

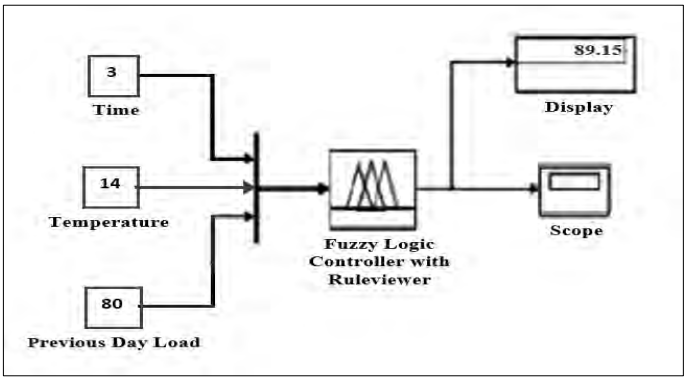

Figure 5: Simulation diagram of Simulink

The Figure 5 shows the Simulink used to simulate. The first input to the FL is time, temperature, and the other is previous load the send to the fuzzy logic controller with rule viewer and output value as shown on display. It is observed from the simulation that for a time of 3am, temperature of 14 ^{0}**C** and the previous load is 80 KW the load is 89.15KW. The Figure 6 demonstrates how the fuzzy system in MATLAB toolbox which works for the sample inputs. For example, it is seen that the low temperature and Medium previous load gives an output of Medium load, similarly for Medium temperature and high previous load the output is Medium load. This can also be seen on rule viewer in Figure 6. The rule viewer below shows the plots of antecedent (time, temperature, Previous Day – Load and Actual Load).

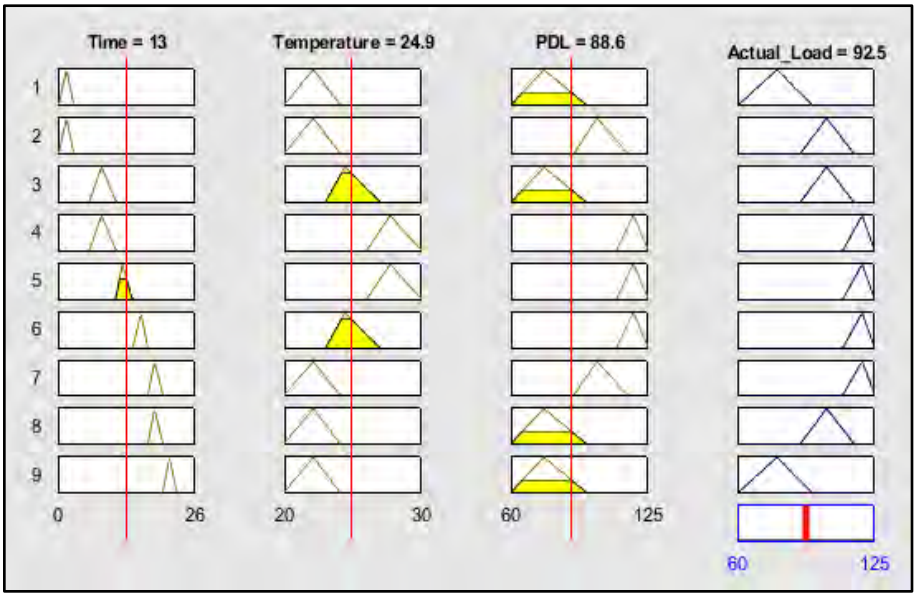

Figure 6: Fuzzy rule viewer

D. Implementation of ANN using MATLAB

Using the historical data as seen in table 1 and saved in an Excel spreadsheet. This data set spans of one day (which are equal 24 hours, The default neural network (NN) fitting toolbox of MATLAB consisting A two –layers feed forward network with five input data and 10 neurons has been used. Activation function is sigmoid for the hidden layer and linear for one output layer. The multilayer perceptron with backpropagation (MLPBP) networks are the most widely used of ANN model. In this paper the MLPBP ANN networks will be optimized in order to predict the values of temperature, next one – day load and previous load on short term load forecasting. The optimized ANN model in MATLAB is shown in Figure 7.

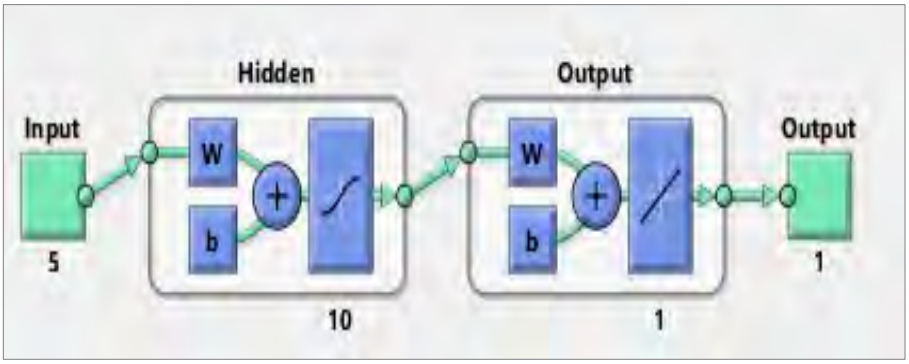

Figure 7: Optimized ANN model in MATLAB

The next step we choose the data which is divided into two Categories one of them is the input of weather variables such as temperature, time and previous data 24 hours load on load forecasting and other is a target for output. Training was set to Seventy Percent (70%), validation was Fifteen Percent (15%), and Testing was Fifteen Percent (15%) number of

hidden neurons ten (10) if the error is high then to minimize the error retrain is done then we can obtain plots of the implement, Train state, Fit and Regression. Figure 8 Shows the ANN performance plot. The total number of epoch produced is 3. It also can be seen that the best validation performance is 15.9635 at epoch 3.

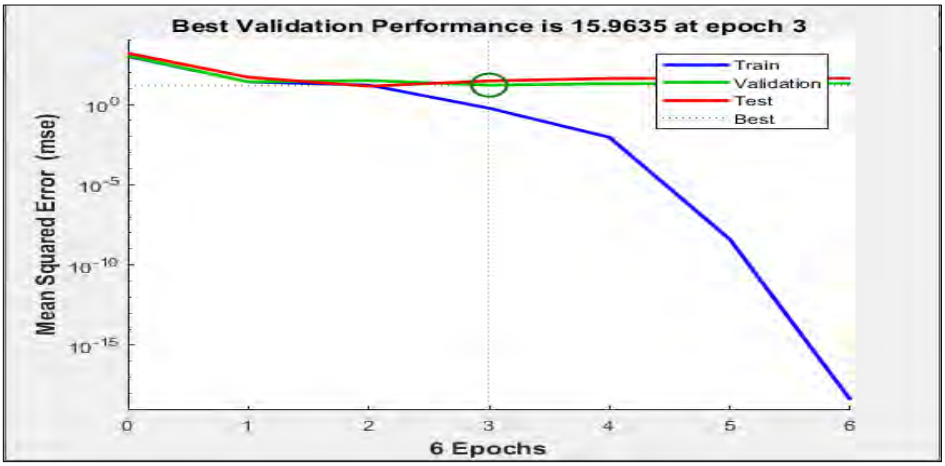

Figure 8: ANN performance plot

Figure 9 illustrates the relationship between the target and outputs are closeness. R value of one $(R=1)$ indicates a perfect. From the regression plot $R=0.9994$ for training, $R=0.9778$ for validation, $R=0.9974$ for testing and $R=0.984$ for all.

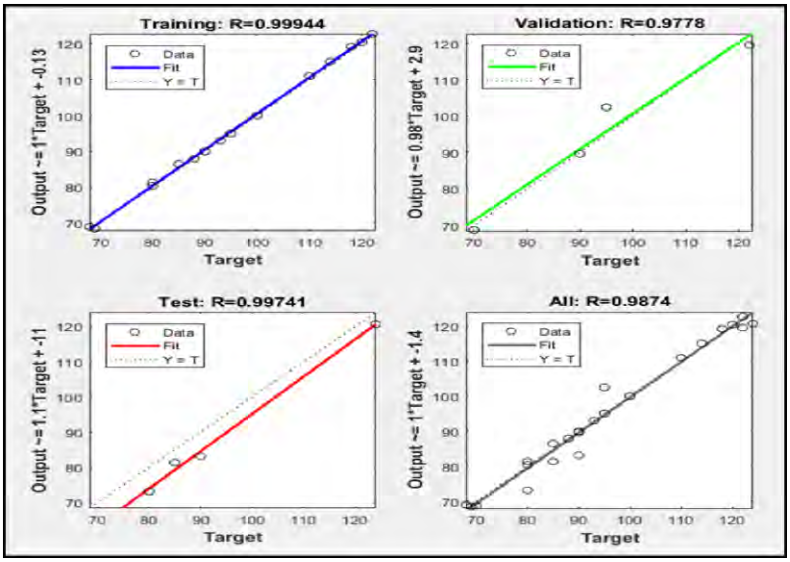

Figure 9: Regression plot

4- Results and Discussion

This work, an Artificial Neural Network (ANN) which is made up of three layers (input layer, a hidden layer, and output layer) was established. The Sigmoid Transfer Function is used for the transfer function between the input and the hidden layer, and the logsig Function for that between the hidden layer and the output layer. The input is number neurons, and the hidden layers must be optimized. Through simulation studies on the short-term load forecasting (24-hours) as shown in Table 3, it is observed that from midnight up to 6.00 am the load is low, and the load increases at 8.00 am. The relationship between load and time of the day is obtained in Table 3. This refers to the rise in temperature at that time. The Table 3 below illustrates the results obtained from data management and analysis were performed using MATLAB in the order obtained the relationship

between forecasted load and Actual load. Through the results show it is very close. Finally, it is observed from Figure 10 that ANN – BP has higher accuracy, faster response and more suitable for the application compare to FL. The % error in the forecast can be calculated as:

$$\% \textbf{ Error} = \frac{\textbf{aclual load} - \textbf{forecast load}}{\textbf{actual load}} \times \textbf{100} \qquad (1)$$

Table 3. Hourly Load Forecast of 2nd January 2016

Input data Short –Term Load Forecast (STLF)					Target	ANN
Time	T (^{0}C)	Previous One – day (kW)	Forecasted load (kW)	FLC (kW)	Target	Output
0.00am	17	70.50	89.50	91.40	68.00	68.00
1.00am	18	70.00	87.10	88.25	69.00	69.00
2.00am	15	69.00	87.10	90.10	70.00	70.12
3.00am	14	80.00	90.50	89.15	85.00	85.11
4.00am	14	75.00	90.50	89.15	80.00	80.10
5.00am	14	90.00	90.50	89.15	85.00	85.08
6.00am	14	88.00	90.50	89.15	80.00	81.57
7.00am	15	89.00	89.00	93.10	80.00	79.73
8.00am	20	95.00	98.00	101.50	95.00	95.84
9.00am	24	95.00	92.50	94.00	95.00	94.75
10.00am	25	105.00	117.00	120.00000	120.00	120.08
11.00am	25	110.00	116.00	118.000	122.00	123.28
12.00pm	26	120.00	117.00	121.00	122.00	122.23
13.00pm	26	125.00	116.00	119.00	124.00	124.23
14.00pm	27	120.00	117.00	120.00	118.00	115.50
15.00pm	26	118.00	115.00	119.00	114.00	114.32
16.00pm	25	115.00	117.00	118.50	110.00	110.32
17.00pm	24	110.00	92.50	94.20	100.00	99.85
18.00pm	24	100.00	92.50	94.20	95.00	94.89

19.00pm.	24	95.00	93.50	95.50	93.00	92.93
20.00pm	21	90.00	92.50	93.25	90.00	90.97
21.00am	20	90.00	92.50	93.25	88.00	90.06
22.00pm	20	00.00	92.00	94.00	90.00	88.54
23.00pm	19	80.00	92.50	93.25	90.00	89.96

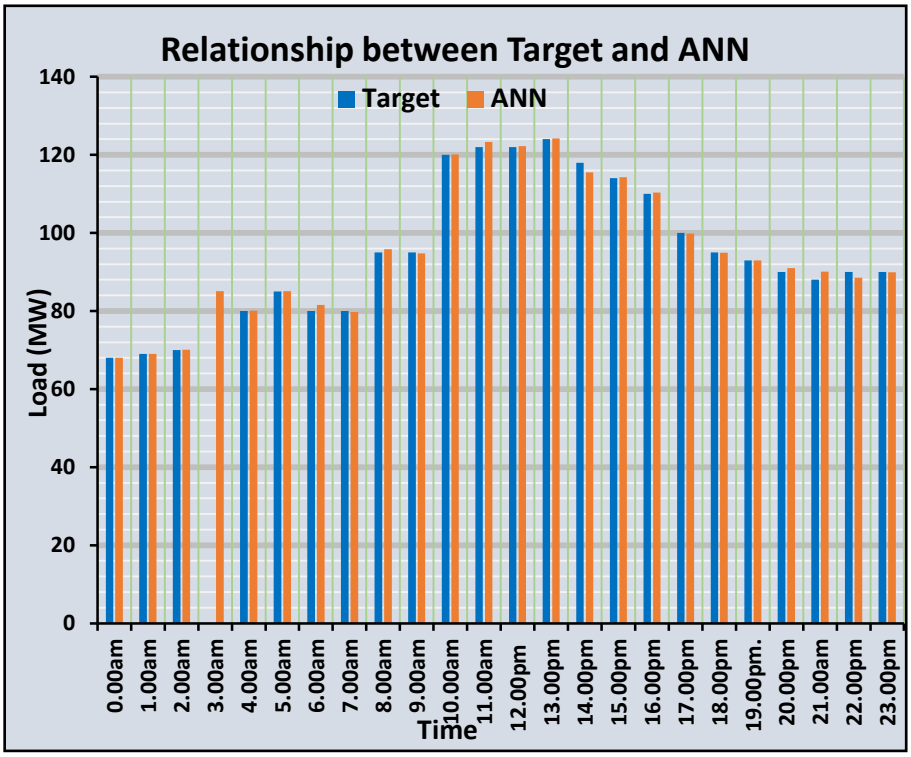

Figure 10: Output ANN

CONCLUSION

The results have shown that ANN is more efficient compared to other traditional load forecasting methods such as Machine learning, artificial intelligence and support vector machines (SVM. In this paper, a methodology for load forecasting using fuzzy logic and artificial neural network approach are presented. This paper has successfully simulated load forecasting with the use of FL and ANN. The results have shown that both ANN and FL can predict forecasting load values. However, ANN gives much more accurate results compared to FL.

ACKNOWLEDGMENT

The authors are grateful to the Universiti Teknikal Malaysia Melaka (UTM) for providing the necessary platform for this research to Centre for Robotics and Industrial Automation (CeRIA), College of Engineering Technology Houn and Higher Institute for Water Technology, Agelat.

REFERENCES

[1] P. Gohil and M. Gupta, "Short Term Load Forecasting Using Fuzzy Logic," Int. J. Eng. Dev. Res., vol. 10, no. 3, pp. 127–130, 2014.

[2] H. A. Abdulqader, "Load Forecasting for Power System Planning and Operation Using Artificial Neural Network At Al Batinah Region Oman," J. Eng. Sci. Technol., vol. 7, no. 4, pp. 498–504, 2012.

[3] A. Danladi, M. I. Puwu, Y. Michael, and B. M. Garkida, "Use of Fuzzy Logic To Investigate Weather Parameter Impact on Electrical Load Based on Short Term Forecasting," Niger. J. Technol., vol. 35, no. 3, pp. 562–567, 2016.

[4] P. GL, K. Sambasivarao, P. Kirsali, and V. Singh, "Short Term Load Forecasting for Uttarakhand using Neural Network and Time Series models," IEEE Int. Conf., vol. On the page, no. S, pp. 1–6, 2014.

[5] S. R and H. A. Al Abdulqader, "Load forecasting for Power System Planning Using Fuzzy-Neural Network," in Proceedings of the World Congress on Engineering and Computer Science, 2012, vol. I.

[6] W. E. I. Sun, "Application of Neural Network Model Based on Combination of Fuzzy Classification and Input Selection in Short Term Load Forecasting," Mach. Learn., no. August, pp. 3153–3156, 2006.

[7] S. M. D. E. Rocco, A. R. Aoki, M. V. Lamar, C. E. P. Brazil, and C. E. P. Brazil, "Load Forecasting Using Artificial Neural Networks and Support Vector Regression," pp. 36–41, 2007.

[8] S. R. Khuntia, J. L. Rueda, and M. A. M. M. van der Meijden, "Forecasting a load of electrical power systems in mid- and long-term horizons: a review," IET Gener. Transm. Distrib., vol. 10, no. 16, pp. 3971–3977, 2016.

[9] M. Mustapha, M. W. Mustafa, S. N. Khalid, I. Abubakar, and H. Shareef, "Classification of electricity load forecasting based on the factors influencing the load consumption and methods used: Anoverview," 2015 IEEE Conf. Energy Conversion, CENCON 2015, pp. 442–447, 2016

[10] K. Bagherifard, O. Ibrahim, S. Izman, N. Janahmadi, and M. Barisamy, "Application of Anfis System in Prediction of Machining Parameters," J. Theor. Appl. Inf. Technol., vol. 33, no. 1, 2011.

Journal of Total Science
Volume (6), Issue (24) (June. 2023)
ISSN: 2518-5799

مجلة العلوم الشاملة
المجلد (6)، العدد (24)، (يونيو2023)
ردمد: 2518-5799

STUDY OF ATMOSPHERIC PRESSURE ELECTRIC ARC BINDING MODES TO THE SURFACE OF HOLLOW THERMOCATHODE

Alkeeb Ahmed M. Mohammed Aljali
Higher Institute of Science and Technology, Suq Aljumuea

NahlaFaiz Abdullah Al Dabagh
Higher Institute of Science and Technology, Tripoli

Abstract. The article presents the results of a study of possible causes of changes in the mode of atmospheric pressure electric arc binding to the surface of a hollow thermocathode. The composition $Ba_3Sc_4O_9$ + W obtained by high-temperature impregnation of tungsten sponge with barium scandatehas been chosen as a cathode material.

It is shown that the reason for the electric arc transition from the diffuse mode of binding to thehollow thermocathode surface into thecontractedone is poisoning of the cathode material by oxygen-containing gases.

Key words: plasmatron; plasma; electric arc; cathode; anode; root.

الخلاصة:

تقدم المقالة نتائج دراسة الأسباب المحتملة للتغيرات في طريقة ارتباط القوس الكهربائي للضغط الجوي بسطح كاثود حراري مجوف. تم اختيار التركيبة $Ba_3Sc_4O_9$ + W التي تم الحصول عليها عن طريق التشريب بدرجة حرارة عالية لإسفنجة التنجستن مع عنصر الباريوم كمادة كاثودية.

يتضح أن سبب انتقال القوس الكهربائي من الوضع المنتشر للربط بسطح الكاثود الحراري المجوف إلى سطح منقبض هو تسمم مادة الكاثود بالغازات المحتوية على الأكسجين.

Introduction

The most promising direction for the further development of industrial plasma equipment is the use of hollow high-emission cathodes [1], which have proven themselves well in the technique of electrovacuum devices, as well as in electroreactive propulsion systems, providing an operational life of several tens of thousands of hours.

Today, cathodic processes in atmospheric pressure arcs with thermoemission electrodes are quite well studied, and the studyresults are summarized in a whole series of works [2, 3]. However, their use is limited by the shortoperational life of the cathode, which is connected with transitions of the binding modes of electric arc from the diffuse form to the contracted one. The arc contraction to the electrode surface leads to an increase in the specific heat fluxes on the cathode and, over time, to burnout of the electrode wall. Traditionally, the existence of two stable forms of arc binding is associated with the existence of bifurcation points in the problem of the thermal balance of the arc cathode. This confirms the result of the theoretical analysis performed by M.S. Benilov, as well as other authors [4-6].

The essential dependence of the emission properties on the atmospheric composition near the emitting surface is a well-known fact. However, until now it has been ignored in the studies devoted to modelling of cathode processes. Most of the authors, when describing the operation of thermoemission cathodes, give tabular data of the work function for different materials and use them in modelling, ignoring the fact that these data have been obtained when testing under deep vacuum conditions. At

the same time, the simplest estimates in the work [7] show that even when using high purity argon [8], at pressures close to atmospheric pressure, the partial pressure of active gases contained in it exceeds critical values for all known thermal emission materials.

The experimental studies of the causes of spontaneous arc transition from one mode to another were conducted mainly for low-current arcs, the research in arcs with currents of the order of 100 A and more remain few.

Purpose

To carry out a numerical experiment to establish the possible causes of changes in the binding mode of the atmospheric pressure electric arc to the surface of the hollow thermocathode.

Research Methodology

Unlike other parts of the plasmatron, which can be protected from direct exposure to electric arc plasma by means of gas or liquid, the electrodes are always in contact with the electric arc. Only on “hot” thermal emission cathodes can all the heat released in the area of the fixed cathode spot be dissipated without noticeable destruction of the cathode.

The cathode is the most heat stressed and the least durable. As for the anode, its operational life can usually exceed the cathodeoperational life. The processesoccurring at the anode are also very complex and diverse, but their study is beyond the scope of this dissertation. The most commonly used thermocathodes in plasmatrons are refractory metals (tungsten, hafnium, zirconium, etc.) with thorium and lanthanum additives that reduce the electron yield. Since tungsten oxidizes intensively, it can be used only if protected by noble gas. In oxidizing environments, hafnium or

zirconium thermocathodes are used that form strong oxide films with good emission properties [9].

Copper or steel cathodes are used in most modern plasmatrons operating at currents from several kiloamperes to tens of kiloamperes. Such cathodes, unlike thermocathodes, cannot operate with a fixed arc root at arc currents over 200 A [10]. Melting point of copper and steel (1083 ºC and 1401 ºC, respectively) does not allow heating them to a temperature at which thermal emission becomes noticeable. Therefore, they are called “cold” as opposed to “hot” thermal emission. The density of heat flows in the arc roots of hollow cathodes is such that it is impossible to remove completely all the heat from their working surface. In order to disperse the heat flow over the working surface and reduce the arc exposure time to a fixed point of the electrode, usually a rapid movement of the arc discharge over its surface with the help of aerodynamic forces or magnetic field is used. However, this does not always give positive results. Especially, when moving the arc at high speed, convective heat transfer between the electrode and the plasma adjacent to it increases sharply. This leads to an increase in thermal loads on the electrodes, increasing their temperature, erosion and reducing efficiency of the plasmatron.

It should be noted that hollow cathodes can be used both at low pressures and high currents (hollow thermocathode) and at high pressures (“cold” cathode).

A separate group is represented by hollow cathodes with placement of several thermal emission inserts along the circumference of a cylindrical electrode [10–15]. Considering that hollow cathodes can be made both of

material with high melting point (Zr, Hf, W, etc.) and of material with low melting point (Cu, etc.), let us briefly consider the most important physical problems related to their operation on the basis of existing theories and hypotheses.

Many physical processes in plasmatrons and cathode operational life are determined by electron emission. Depending on the cathode temperature, pressure, electric field strength and a number of other conditions, different forms of emission can dominate. If the cathode operates at high temperatures, thermionic emission plays the determining part. In these conditions, the thermal emission current density is determined by the Richardson–Dashmanequation:

$$j_{ek} = A_r \, T_k^2 \, e^{-\frac{e\varphi_e}{kT_k}},$$

where A_r is the Richardson constant, which for the most pure metals, is equal to $60 \ \mathrm{A \cdot cm^{-2} \cdot K^{-2}}$; in the case of composites (base metal + emitter substance) $A_r$is by one or two orders of magnitude smaller; φ is the electron work function (potential) from the cathode; k is the Boltzmann constant; T_K– absolutetemperature.

Almost all researchers ignore the fact that the emission properties of cathode materials change depending on the composition of gas in the electrode sheath of plasmatrons. For example, most authors give tables with values of electron work functionand use them in further calculations, not taking into account that these data have been obtained when testing materials under ultrahigh vacuum conditions. At the same time, it is known

that for any materials the emission properties deteriorate even at insignificant presence of active oxygen and water vapour in the electrode sheath, and at increase of critical values of their partial pressure – emissiondrops dozens of times.

In practice, ignoring the dependence of work function on atmospheric composition leads to the following. In order to maintain the combustion of the arc, a certain level of electron emission is required. Elementary analysis shows that when inert gases of technical purification are used in plasmatrons, the content of poisoning impurities in the cathode sheath exceeds the critical values for all known thermoemission materials. Since the work of electron output from the poisoned cathode surface is much higher than the value for high vacuum conditions, the arc burning becomes possible only at strong compression of the arc root on the cathode. This leads to increase of specific heat fluxes by 5...10 times, causing overheating of the emitter (sometimes up to melting temperature) and, accordingly, to catastrophic erosion of the cathode.

In most cases, when studying the emission mechanism, the cathode surface is assumed to be smooth, but in fact it has inhomogeneities, contaminations, which have a strong influence on the course of emission and erosion processes. The researches of Ecker G. [16] allowed to find that near the cathode with a rough surface there is inhomogeneity of the electric field and increase of its intensity, which leads to reduction of the work function (Schottky effect), as well as explosions of microspikes occur. When the heterogeneity factor is taken into account, it is assumed that all cathode points are in the same conditions with respect to the generated positive charge. However, the analysis shows that there is a localized

region on the cathode surface that is characterized by a higher value of the potential barrier decrease and increased charge density, which contributes to the increase of emission from this region and formation of the cathode spot. In order to estimate the emission, it is necessary to know how the temperature is distributed over the cathode surface. This question has been investigated by a number of authors, including the author [7].

Thus, in addition to the emission properties of the cathode material, such factors as the topology of the electric field near the cathode surface, the nature of the temperature distribution on the emission surface have an influence on the emission character, which makes it possible to control the emission processes and influence the operational life of the cathode.

Reference values of the work function for different emission materials have been obtained by testing the samples under vacuum conditions, which do not correspond to the conditions of the emitter operation under atmospheric pressure.

Reliable determination of the values of the electron work function for different thermocathode samples and determination of dependences of the work function on the partial pressure is possible only under the conditions of full-scale tests. However, the possibility of conducting such tests is significantly limited by the complexity of compliance with the necessary experimental conditions, as well as by economic factors.

In the course of preliminary experiments in the work [7], the possibility of creating conditions close to those of the hollow cathode in a sealed volume without gas flow was shown. The plasma state spectra and voltampere dependences of the discharges were chosen as characteristics

for comparing the operation of the emitters with and without gas flow. For this purpose, we made models of hollow cathodes with interchangeable diaphragms and metal and glass housings, as well as a model of a gas diode in a glass bulb (Fig. 1).

The emitter block design of these models was identical and corresponded to the real hollow cathode. These models were used to perform spectral analysis of the plasma column adjacent to the emitter. In order to compare the discharge plasma states in the flowing hollow cathode and the non-flowing diode, full spectra in the wavelength range of 390-830 nm (Fig. 2) were compared using the HR-4000 spectrometer.

Fig. 3 compares the line intensities of excited atoms of the protective noble gas with energy levels close to the ionization potential. A sufficiently good coincidence of the intensities of the lines in the full spectra indicates the proximity of gas compositions and its impurities in the plasma of two discharges. A comparison of the line intensities of excited atoms with energy levels close to the ionization potential shows the identity of the plasma states in the flowing and non-flowing discharges.

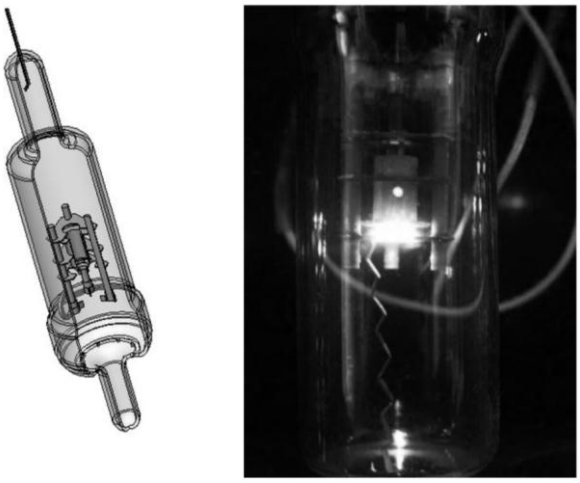

a b

Figure 1 –Model of the hollow cathode in a sealed bulb used for the operational life testing

a – 3D model; b –model during the tests

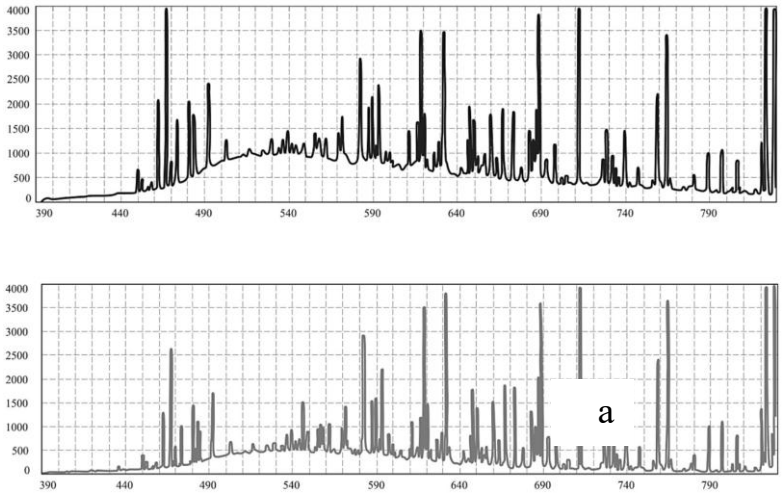

b

Figure 2 – Fullplasma spectra in the hollow cathode and model:

a – hollowcathode; b –non–flowing diode

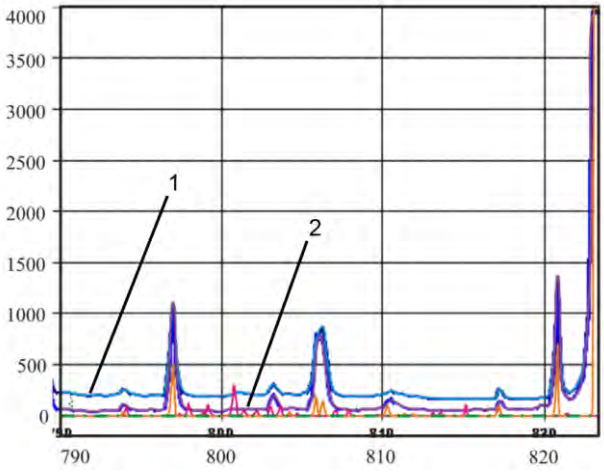

Figure 3 – Lineintensities of excited atoms:

1 – flowinghollow cathode; 2 – non-flowing diode (model)

To conduct the emitters operational life testing, a number of models of hollow cathodes in sealed quartz glass bulbs were made. The tests were carried out for scandalous emitters in diode mode. Xenon with pressure from 20 to 200 Torr and argon with atmospheric pressure were used as the working gas in the bulbs. The geometry of the discharge gap, the size of the emitter, and the current density repeated the conditions of the real design of the cathode assembly.

In xenon-filled bulbs at pressures from 10 to 100 Torr, the emitter operated in the diffuse arc binding mode (see Fig. 4) with approximately constant voltage. At pressures above 100 Torr, the cathode went into the spot mode of operation with unstable, jump-like change of voltage in the discharge. This mode is accompanied by local overheating of the emitter surface at the binding point with obvious signs of erosion. When filling the bulbs, we used xenon grade 5.8 according to TU 2114-003-39791733-2002 with oxygen-containing impurities at or below 0.3 ppm.

At pressure in the bulb equal to 100 Torr, partial pressure of active gases will be $P_{nap} \approx 4 \cdot 10^{-3}$ Pa, which is almost equal to the critical partial pressure for the composition used in the manufacture of the emitter volume fraction of $Ba_3Sc_4O_{9B}$ 30 %+ volume fraction of W in 70% ($5 \cdot 10^{-3}$Pa). Thus, in the conducted experiments, the transition from the diffusion-bound mode to the mode with the contracted arc is associated with exceeding of the critical level of partial pressure of active gases and related poisoning of the emitter.

The same mechanism should act at higher pressures.

Therefore, conclusions made in many works on the basis of experimental studies about impossibility to implement the mode with diffusion binding at pressures close to atmospheric are incorrect. Increasing the operating pressure while maintaining the gas composition leads to a proportional increase in the partial pressure of active gases. Consequently, for operation with diffusion binding it is necessary to use gas of higher degree of purification.

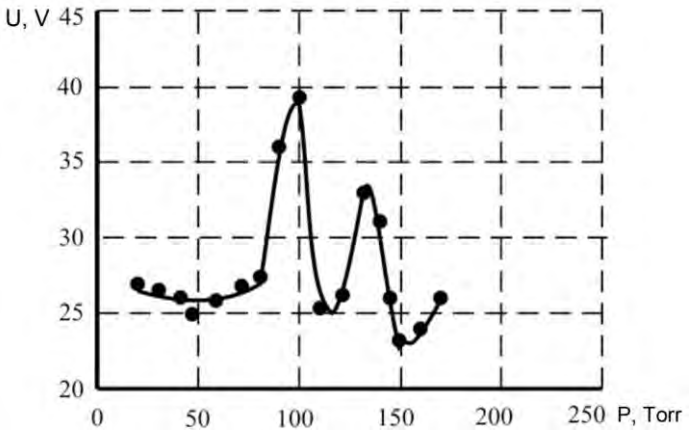

Figure 4 – Dependence of arc voltage on xenon pressure in the model of cathode

assembly with a hollow-cathode [7]

When determining theemitters operational life, in order to reduce the time of the experiment, theaccelerated tests were carried out. For this purpose, after degassing, bulbs were filled with atmospheric pressure argon (the highest grade according to GOST 10157-79) with the partial pressure of oxygen-containing gases at 0.7 Pa, i.e. higher than the critical partial pressure for the emitter from the volume fraction $Ba_3Sc_4O_{9B}$ 30% of 30% + volume fraction W of 70%.

During the experiments, automatic control of discharge current parameters was carried out. After arc initiation, the models worked in continuous mode. Uninterrupted power sources provided automatic arc ignition in case of abnormal shutdowns. Up to 5 models were tested simultaneously. Tests were conducted until the emitters were completely exhausted and the arc was interrupted. As a result of the tests, it was found that the time of continuous operation of the emitters, when working in an argon atmosphere at a pressure of 0.1 MPa,comprised from 3000 to 3200 hours.

The samples operated in xenon atmosphere at the pressure, which provided the subcritical level of partial pressure of oxygen-containing gases, worked more than 10000 hours in the mode with diffuse arc binding.

Returning to the question of atmospheric pressure electric arc binding modes to the surface of a hollowthermocathode, from the author's point of view, the transition from diffuse binding to contracted for thermionic emission cathodes can be explained by an increase in the electron work

function from the cathode surface as a result of its poisoning with oxygen-containing gases, as indicated by the results of the above described operational life testing. A certain level of electron emission is necessary to keep the arc burning; if this does not happen, arc burning becomes possible only when the spot is strongly compressed. The studies of various emission materials have shown their extreme sensitivity to oxygen-containing gases. So in the work [7], it is shown that on average the emitter poisoning threshold lies within the range of air pressures $1\cdot10^{-3}...1\cdot10^{-2}$Pa, even the use of argon as a protective gas does not provide gas dynamic protection of the cathode. According to GOST $10157-79$, the oxygen volume fraction in argon of the first grade shall not exceed 0.002%, the highest – $0{,}0007\%$, special purity – $0{,}0005\%$. When using such protective gases at a working pressure of 0.1 MPa, the partial pressure of oxygen near the emitter will be 2.0, 0.7 and 0.5 Pa, respectively.

This pressure of active gases exceeds the critical levels for all existing thermionic materials, see Fig. 5.

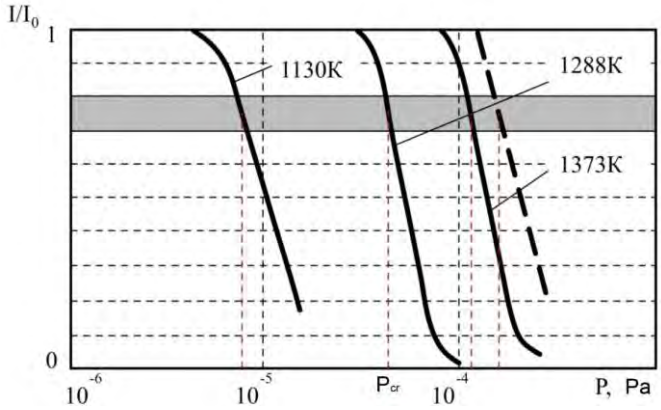

Figure 5 –Changes of emission current depending on air pressure (W-Ba):

P – airpressure, I_0– initialvalue of current intensity, I–currentintensity after “poisoning” of the emitter

The essential dependence of the emission properties on the atmospheric composition near the emitting surface is a well-known fact. However, until now it has been ignored in the studies devoted to modeling of cathode processes. Most of the authors, when describing the operation of thermal emission cathodes, give tabular data of the work function for different materials and use them in modeling, ignoring the fact that these data were obtained when testing under deep vacuum conditions. At the same time, the simplest estimates in the work [7] show that even when using high-purity argon [8], at pressures close to atmospheric pressure, the partial pressure of active gases contained in it exceeds the critical values for all known thermal emission materials.

In order to confirm the assumption about the possible reasons of changing the binding mode, the following numerical experiment was carried out in the present work: the cylindrical hollow cathode has dimensions: 5x1 mm, length 7 mm, the distance from the flat copper anode is 10 mm. The composition $Ba_3Sc_4O_9$ + W was chosen as the cathode material. Such cathodes are made by high-temperature impregnation of tungsten sponge with barium scandate. This emitter passed vacuum testing for emission, temperature, resource, and poisoning properties [17]. Fig. 6 shows dependence of the work function for the selected material on temperature.

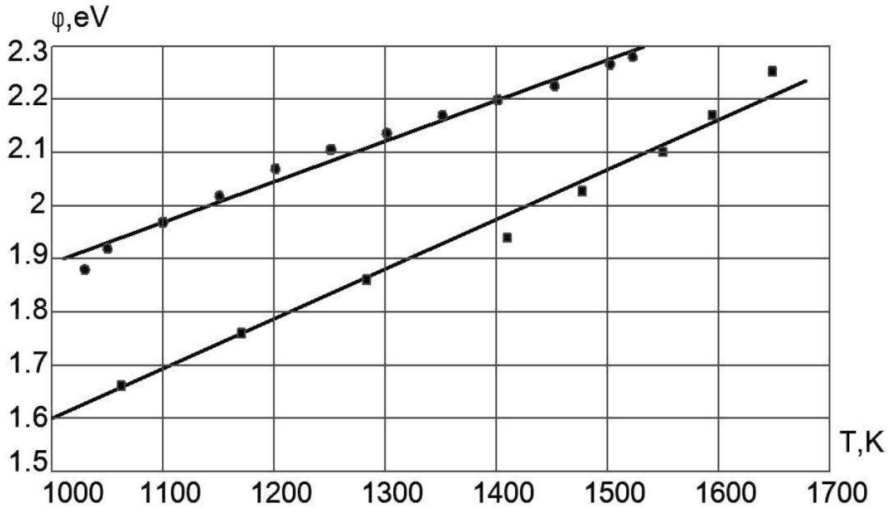

Figure 6 – Dependenceof the work function on emitter temperature for samples from different batches [18]

In the calculations,it is set the flow rate of protective gas (argon) through the annular slot of 5 mm, 10 L/min and through the cathode cavity – 2 L/min. The temperature at the outer end of the cathode and at the lower surface of the anode is fixed at 300 K.

The mathematical description was based on the magnetogasdynamic approach to plasma as a continuous medium based on gas dynamics equations, Maxwell equations and relations for thermodynamic parameters in ionized gas with the following assumptions:

- The plasma is assumed to be quasi-neutral: $n_e = n$or $n_e = \Sigma (Z_a n_a)_a$in the case of multicharged ions or multicomponent plasma. Here n_e, $n$are concentrations of electrons and ions, respectively.
- The plasma is thermally equilibrium – thetemperature of all groups of

particles is the same.

- The gas composition in thermodynamic equilibrium can be determined through the thermodynamic parameters of the gas. Ionization equilibrium in plasma is described on the basis of the Saha equation:

$$n_e\left(\frac{n_r}{n_{r-1}}\right)=2\frac{g_r}{g_{r-1}}\left(\frac{2\pi m_e kT_e}{h^2}\right)^{3/2}\exp\left(-\frac{U_I-\Delta U_I}{kT_e}\right),$$

where g is the statistical sum; m_e is the electron mass; T is the absolute temperature of the gas particles; U is the energy required to remove electrons from a neutral atom.

- In plasma, Ohm's law is valid in its simplest form: $\bar{j}=\sigma\bar{E}$, here j– emission current density; σ– gasconductivity; E– electricfield strength
- The expression for pressure can be written as the sum of pressures of individual components:

$$p=\sum_a n_a kT_a+n_e kT_e,$$

where k is Boltzmann constant.

- The mechanism of electron emission is assumed to be thermo–emission following Richardson's law

Results of the study and their discussion

The problem was solved in two stages: firstly, the stationary problem for an arc burning in an atmosphere of pure argon was solved. Then, using this solution, a nonstationary problem with a gradual increase in the air content in the plasma-forming gas was considered as an initial one. The dosed introduction of atmospheric air occurred using a point source problem with a flow rate of 0.01 g/s. The time step was chosen as $1e^{-6}$s.

In pure argon, the arc burned steadily in the diffuse binding mode (Fig. 7).

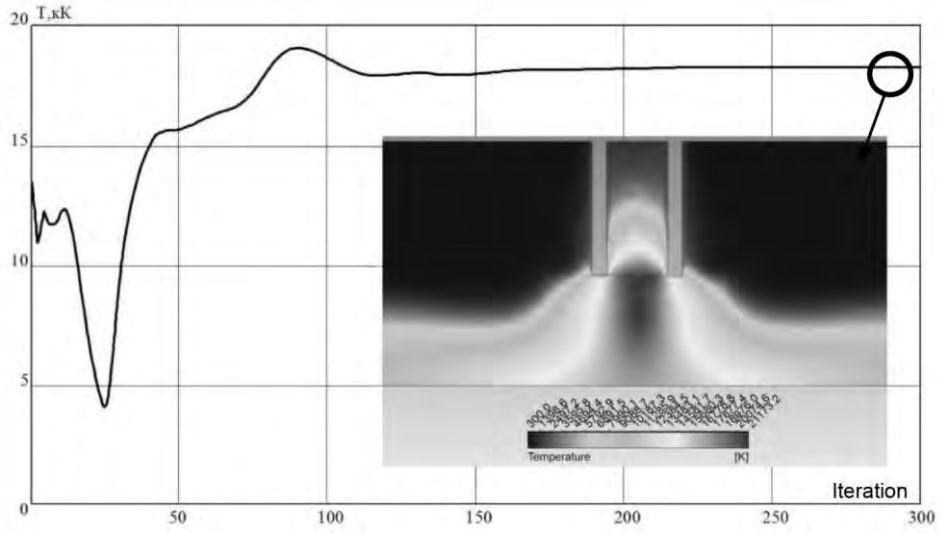

Figure 7 – Electricarc in the diffuse binding mode at stationary setting up the problem

The same mode was maintained at the initial stage of solving the nonstationary problem. However, with further increase in the air content in the plasma-forming gas, a transition to the contractedform of arc binding

occurred (Fig. 8). The arc was randomly bound at first to the inner surface of the emitter, and then it was fixed at the end of the hollow cathode.

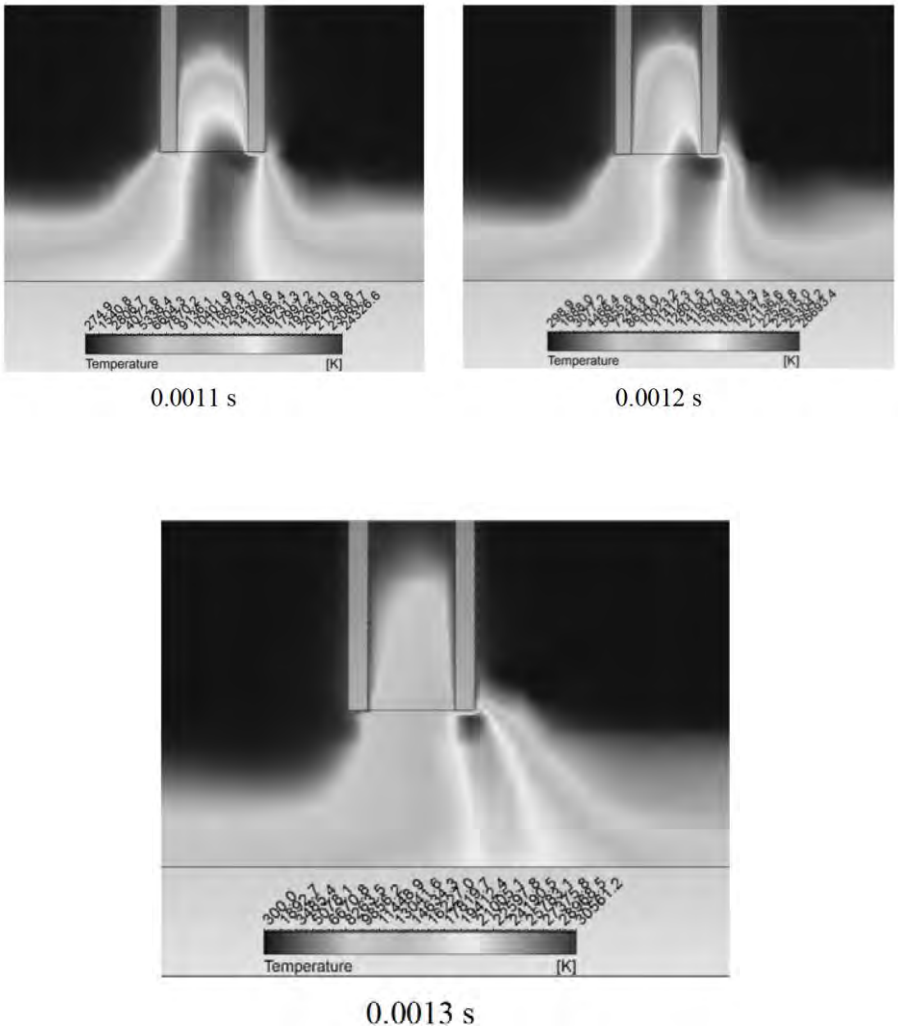

Figure 8 – Changeof arc binding mode in time following “poisoning” of the cathode by atmospheric air

The simulation results coincide with the operating modes of hollow cathodes with atmospheric pressure arcs observed in the experiments and can indicate that the main reason for the transition to a contracted arc in this case is poisoning of the emitter material.

Traditionally, hollow thermoemission cathodes, in contrast to cold cathodes, are limited in use when operating at atmospheric pressure. This is explained by impossibility to compensate the atmospheric pressure by pressure of plasma column inside the cathode cavity, which leads to arc extrusion to the cathode ends with subsequent reattachment to the outer surface of the cathode, but the obtained result allows to connect this process with insufficient level of emission from the cathode surface to keep the arc in the diffusion mode.

From a practical point of view, this allows us to consider the creation of workable designs of plasma generators with hollow thermionic cathodes for operation at high pressure. At achievable degree of purification of argon (about $1\cdot10^{-3}$ Pa at partial air pressure), this requires use of cathode materials providing a sufficient level of emission. Such materials can be, for example, compositions of the type W + $Ba_xMe_yMe_zO_v$ (Me – Sc, Sr, Hf, Zr), some of which keep high emission properties up to values $1\cdot10^{-2}$ Pa at partial air pressure

Conclusions

1. It is confirmed that the reason forthe electric arc transition from the diffuse mode of binding to the hollow thermocathode surface into the contracted mode is “poisoning” of cathode material by oxygen–containing gases.

2. The obtained result makes it possible to use the pattern of temperature and current density distribution in the cathode sheath as a criterion for estimating the acceptable values of the partial pressure of oxygen-containing gases. Thus, at the stage of design of cathode assembly using the proposed criterion, during numerical experiments, it is possible to determine geometric parameters of cathode assembly and flow modes of protective and plasma-forming gas, allowing to provide diffusive binding mode as the most sparing mode of cathode operation, even at decrease of emission current to values $0.7...0.8$ from emission current in vacuum.

3. Analysis of operational life testing of hollow cathodes showed the possibility of application of high-emission hollow cathodes at atmospheric pressure under condition of providing necessary parameters of the gas medium in the cathodesheath.

Refrences

1. Imitatsiya teplovykh nagruzok i sostava gazovoy sredy pri sverkhzvukovykh i giperzvukovykh skorostyakh poleta v nazemnykh ispytaniyakh modeley i elementov konstruktsiy letatelnykh apparatov s pomoshch'yu plazmotronov [Tekst] / S.I. Plankovskiy, Ye.V. Tsegelnik, Ye.K. Ostrovskiy, D.A. Brega // Otkrytyye informatsionnyye i kompyuternyye integrirovannyye tekhnologii: sb. nauch. tr. Nats. aerokosm. un-ta im. N.Ye. Zhukovskogo «KHAI».– Vyp. 45. – KH., 2010. – S. 109 – 115.
2. Prielektrodnyie protsessy v dugovykh razryadakh [Tekst] / M.F. Zhukov, N.P. Kozlov, A.V. Pustogarov i dr. – Novosibirsk: Nauka, 1982. – 158 s.
3. Matematicheskoye modelirovaniye katodnykh protsessov. Nizkotemperaturnaya plazma. [Tekst] / A.M. Zimin, I.P. Nazarenko, I.G. Panevin, V.I. Khvesyuk. – Novosi- birsk: Nauka, 1992. Vyp. 10. – 197 s.
4. Teoriya i raschet prielektrodnykh protsessov. Nizkotemperaturnaya plazma. [Tekst] / I.G. Panevin, V.I. Khvesyuk, I.P. Nazarenko i dr. – Novosibirsk: Nauka, 1992. Vyp. 10. 197 s.
5. Mesyats, G. A. Cathode phenomena in a vacuum discharge: the breakdown, the spark and the arc [Tekst] / G.A. Mesyats. – Moscow: Nauka, 2000. 400 p.
6. Mitrofanov, N.K. Dve formy privyazki atmosfernoy dugi postoyannogo toka v argone k termoemissionnomu katodu [Tekst]/ N.K. Mitrofanov,

S.M. Shkol'nik // Zhurnal tekhnicheskoy fiziki. Sankt-Peterburg. – 2007. – S. 34-44.

7. Plankovskiy, S.I. Nauchnyye osnovy sozdaniya vysokoresursnykh termoemissionnykh katodnykh uzlov oborudovaniya dlya plazmennoy obrabotki materialov [Tekst]: diss… d-ra tekhn. nauk: 05.03.07 / Plankovskiy Sergey Igorevich. – Kharkov, 2009. – 333 s.

8. GOST 10157-79. Bibliograficheskaya zapis'. Bibliograficheskoye opisaniye. Argon gazoobraznyy i zhidkiy. Tekhnicheskiye usloviya [Tekst]. – M.: Izd-vo standartov, 2094. – 21 s.

9. Bolotov, A.V. Elektrotekhnologicheskiye ustanovki [Tekst]/ A.V. Bolotov, G.N. Shepel.– M.: Vyssh. shk., 1988. – 336 s.

10. Chekalin, E.K. Dinamicheskiye svoystva nestatsionarnykh katodnykh pyaten v shirokom diapazone davleniy gaza [Tekst] / E.K. Chekalin, K.V. Chaykovskiy// Tez. dokl. XI Vsesoyuz. konf. «Generatory nizkotemperaturnoy plazmy». – ch.2 – Novosibirsk. – 1989. – S. 99-100.

11. Sharakhovskiy, L.I. Chislennoye modelirovaniye protsessa erozii mednogo katoda s ispolzovaniyem modeli ekvivalentnogo teplovogo istochnika [Tekst] /L.I. Sharakhovskiy, V.N. Borisyuk // Tezisy dokl. X Vsesoyuz. konferentsii po generatoram nizkotemperaturnoy plazmy. – Minsk, 1986., ch.1. – S. 79-80.

12. Korsunov, K.A. Nauchnyie osnovy povysheniya effektivnosti tekhnologicheskikh plazmotronov [Tekst]: diss … doktora tekhn. nauk: 05.03.07 /

13. Korsunov Konstantin Anatoliyevich. – Lugansk, 2010. – 310 s. 13. Yasko, O. I. Elektricheskaya duga v plazmotrone [Tekst]/ O.I. Yasko. – Minsk: Nauka i tekhnika, 1977. – 151 s.

14. Lukashov, V.P. Elektrodugovyye plazmotrony promyshlennogo naznacheniya [Tekst] / V.P. Lukashov, A.N. Timoshevskiy // Plazmokhimiya – 90, CH.2. M.: – INKHS AN SSSR, 1990. –S.303-336.

15. Erozionnaya stoykost elektrodov metallurgicheskikh plazmotronov [Tekst] / Zamulo N.I., Latash YU.V., Zabarilo O.S., Melnik G.A. i dr. Probl. spets. metallurgii. – 1989. – Vyp.2 – S.76-83.

16. Zakharkin, R.Ya. Vodorodnyy plazmotron moshchnostu 2 MVt [Tekst] / R.YA. Zakharkin, A.V. Pustogarov, B.S. Gavryushchenko i dr. // Tez. dokl. VI Vsesoyuz. konf. po generatoram nizkotemperaturnoy plazmy. – Frunze: Ilim, 1974. – S. 137-140.

17. Koshelev, M.M. Resursni vyprobuvannya emiteriv slabkostrumovykh katodiv [Tekst] / M.M. Koshelev // Aviatsiyno-kosmichna tekhnika i tekhnolohiya. – 2007. - №7(43). – S. 78-90.

18. Predvaritel'nyye ispytaniya W-Ba-Sc emitterov katodov ERD [Tekst] / A.V Loyan, N.N. Koshelev, Ye.P. Soloninko, Ye.G. Ageyeva. // Dvigateli i energoustanovki aerokosmicheskikh letatelnykh apparatov. – 2010. - №8 (75). – S. 68-71.

Journal of Total Science
Volume (6), Issue (24) (June. 2023)
ISSN: 2518-5799

مجلة العلوم الشاملة
المجلد (6)، العدد (24)، (يونيو2023)
ردمد: 2518-5799

Prediction of Asphaltene Precipitation During Gas Injection Enhanced Oil Recovery

Mohamed E. Tarrum [1]Chemical Engineering Department, Higher Institute for Science and Technology Souq- Al-Khamies, Libya

Almabruk F. Almeslati [2,3]Chemical Engineering Department, Al-Mergib University, Algaraboli, Libya

Awad E. Gashgesh [2,3]Chemical Engineering Department, Al-Mergib University, Algaraboli, Libya

Abdulbaset M. Elarbie [4]Chemical Engineering Department, Higher Institute for Science and Technology Awlad Ali, Tarhona Libya

ABSTRACT

Tertiary recovery, the third stage of production, was that obtained after the secondary oil recovery is a process by which water is injected into a reservoir to obtain additional oil recovery . Tertiary processes used miscible gases to displace additional oil after the secondary recovery process became uneconomical.

Several gases have been injected in hydrocarbon reservoirs as part of Enhanced Oil Recovery process. The combined mobility of the two phases is less than of the injected gas alone, and thus the mobility ratio in the process is improved.

Natural gas is a mixture of hydrocarbons and a few non-hydrocarbons.

Asphaltene precipitation is a well-Known problem in the oil industry. To prevent this problem, it is important to predict the temperature and pressure under which asphaltenes will form. Asphaltene precipitation upon mixing of oil with gas for Enhanced Oil Recovery applications can be determine experimentally.

In this work asphaltene precipitation conditions have been predicted using HYSYS software Refractive index technique, PVT sim software and thermodynamic calculations.

The main objective of this study is to investigate the problems associated with water and gas alternating process. Investigation of asphaltene precipitation as injection gas contacts oil.

Results obtained to determine asphaltene precipitation using computer software PVT SIM and HYSYS showed good agreement with data from literature and for the selected oil.

1. Introduction

Purpose of WAG injection

The purpose of WAG injection is to improve oil recovery, by both increasing the macroscopic and microscopic sweep efficiency and for pressure maintenance.

Thus, a combination of the improved microscopic displacement efficiency by gas injection with the improved macroscopic displacement efficiency by water injection, improved oil recovery can be achieved.

Problems associated with WAG Asphaltenes precipitation

Asphaltene precipitation may occur under various thermally or non thermally enhanced oil recovery schemes and miscible gas injection which involves the injection of a gas that is miscible with the reservoir oil under reservoir conditions of pressure and temperature. Asphaltenes are high-molecular-weight organic fractions of crude oils that are soluble in toluene, but insoluble in alkanes (e.g., n-heptane and n-pentanes). Asphaltenes tend to remain in solution or in colloidal suspension under reservoir temperature and pressure conditions. They may start to precipitate once the colloidal suspension is destabilized, which is caused by changes in temperature and/or pressure during primary depletion. Asphaltenes have also been reported to become unstable as a result of blending (commingling) fluid streams, as well as by gas injection during EOR operations. Asphaltenes can also become unstable when produced injection gas contacts the oil. Asphaltenes deposition in reservoirs happen when asphaltenes flocculate by depressurizing the oil. The second reason

for asphaltenes deposition is when solvent are used to displace oil in (EOR).

Asphaltenes only become a problem during production when they are unstable.

problems Associated with Asphaltene precipitation

Recognized by light oils with small amounts of asphaltenes are more likely to cause problems during production than heavy oil with larger amounts of material in the asphaltene fraction. The heavier oil also contains plenty of intermediate components that are good asphaltene solvents whereas the light oil may consists largely of paraffinic materials in which, by definition, asphaltenes have very limited solubility. Asphaltenes in heavier oils can also cause problems if they are destabilized by mixing with another crude oil during transportation or by other steps in oil processing.

Unstable asphaltenes can form a separate phase that might plug the oil –bearing rock formation near a well. They can also aggregate at/water interfaces where they stabilize water–oil emulsions or at oil/solid interfaces where they can alter surface wetting properties or accumulate and plug well bores and flow lines. The first step toward predicting and avoiding any of these problems is knowing how to evaluate asphaltene stability.

Two dead crude oils (oils A,B) from different sources were used in this study. In order to confirm the obtained results, experimental results from literature were utilized for comparison.

A commercial package software's (HYSYS) and PVT sim were utilized to determine Asphaltene Precipitation Conditions.

2. Problems Associated With WAG Process

WAG in this process water and gas are injected, the purpose of WAG injection is to improve oil recovery.

The major problems in the evaluation of WAG is :-

2.1 Asphaltene Precipitation Conditions

Asphaltenes have been reported to become unstable as a result of blending fluid streams, as well as by gas injection during EOR operations.

Asphaltenes can also become unstable when produced injection gas contacts the oil.

2.2 Calculation of Asphaltene precipitation conditions

When oil (liquid phase) and gas (vapor phase) are mixed the mixture can be either:

liquid phase , vapor phase , Two phase

Crude oil A

The crude oil composition obtained from gas chromatograph analysis as shown in table (2.1) below.

Table 2.1 Composition of oil A

component	Mole %	Mol wt	Liquid density kg/m³	component	Mole %	Mol wt	Liquid density kg/m³
N2	0.32	28.014		C14	2.25	190	836.0000
CO2	2.29	44.010		C15	2.14	206	841.9999

H2S	0.01	34.080		C16	1.79	222	848.9999
C1	17.67	16.043		C17	1.47	237	845.0000
C2	5.25	30.070		C18	1.32	251	847.9999
C3	6.14	44.097		C19	1.26	263	857.9999
iC4	1.91	58.124		C20	1.15	275	862.9999
nC4	4.72	58.124		C21	0.99	291	867.9999
iC5	2.51	72.151		C22	0.89	305	873.0000
nC5	3.33	72.151		C23	0.78	318	876.9999
C6	5.00	86.178	663.9999	C24	0.70	331	880.9999
C7	5.12	96	737.9999	C25	0. 62	345	884.9999
C8	5.53	107	764.9999	C26	0. 58	359	888.9999
C9	4.84	121	781.0000	C27	0. 53	374	892.9999
C10	4.48	134	791.9999	C28	0. 49	388	897.0000
C11	3.78	147	795.9999	C29	0. 46	402	899.9999
C12	3.09	161	809.9999	C30+	3.83	595	965.0000
C13	2.78	175	824.9999				

The conditions of selected reservoir are 397 K and 30510 KPa. API is 40.4

Injection gas for oil A.

Table 2.2 Composition of the injection gas.

component	Mole %	Mol wt	Liquid density kg/m³
N2	0. 59	28.014	
CO2	5.03	44.010	
H2S	0.03	34.080	
C1	65.76	16.043	
C2	11.32	30.070	
C3	8.58	44.097	
iC4	2.16	58.124	
nC4	3.62	58.124	
iC5	1.24	72.151	
nC5	1.14	72.151	
C6	0. 51	86.178	663.9999
C7	0.03	96	737.9999

Crude oil B

Table 2.3 presents the concentration of the pure components and pseudo-hydrocarbon components for the selected oil. It also gives the mole fraction, molecular weight (M_W), and density(ρ) of the hydrocarbon residue.

The conditions of the selected reservoir are 417 K and 39768 KPa

Table 2.3 Composition of oil B

component	Mole %	Mol wt	Liquid density kg/m³	component	Mole %	Mol wt	Liquid density kg/m³
N2	0.03	28.014		C12	4.33	161	809.9999
CO2	0.64	44.010		C13	4.31	175	824.9999
C1	4.82	16.043		C14	4.3	190	836.0000
C2	2.57	30.070		C15	4.7	206	841.9999
C3	2.25	44.097		C16	4.17	222	848.9999
iC4	1.14	58.124		C17	4.21	237	845.0000
nC4	2.12	58.124		C18	3.71	251	847.9999
iC5	1.73	72.151		C19	3.52	263	857.9999
nC5	1.99	72.151		C20	3.43	275	862.9999
C6	3.91	86.178	663.9999	C21	3.97	291	867.9999
C7	0.78	96	737.9999	C22	2.45	305	873.0000
C8	2.27	107	764.9999	C23	3.08	318	876.9999
C9	2.95	121	781.0000	C24	2.69	331	880.9999
C10	4.57	134	791.9999	C25	2.74	345	884.9999
C11	3.88	147	795.9999	C26+	12.731	400	886.000

Injection gas for oil B

Table 2.4 Composition of the injection gas.

Component	Mol %	Mol wt	Liquid density kg/m³
N_2	0.935	28.014	
C1	83.248	16.043	
C2	13.973	30.070	
C3	1.593	44.097	
iC4	0.018	58.124	
nC4	0.184	58.124	
iC5	0.028	72.151	
nC5	0.018	72.151	
C6	0.004	86.178	663.9999
C7	0.0001	96	737.9999

3. Results and Discussion:

In this work asphaltene precipitation conditions (onset asphaltene precipitation pressure) and bubble point pressure were determined for two different oils.

Determined onset asphaltene pressure and bubble point pressure were compared to experimental data from literature for one oil only.

Figure 2.3. For the reservoir oil B as noted, the OAP pressure is significantly higher than the bubble point (BP) pressure. It is also noted

that the difference between the OAP and BP pressures increases as temperature decreases from 350 to 320 °K. The larger the difference the larger the instability. As expected, the maximum amount of asphaltene occurs very near the bubble point pressure. In addition, it is predicted that the amount of asphaltene increases with a decrease in temperatures

As can be seen, the on set asphaltene precipitation pressure was much higher than the corresponding bubble point pressure for a given concentration of injection gas.

As noted from Figures 2.4 and 2.5, the difference between the on set asphaltene precipitation pressure and the bubble point pressure increases with increasing injection gas concentration. Asphaltenes are becoming more unstable with increasing injection gas. It can be inferred from the asphltene lines that the maximum amount of asphaltene formation occurring at the bubble point of the oil/gas mixtures will increase with increasing gas concentration.

The EOS prediction of the saturation pressures for the swelling experiment is compared to the experiment results in Figure 2.4and demonstrated a good match.

PVT sim predictions for the reservoir oil – injection solvent asphaltene behavior are compared to the experimental data in the form of a P-X diagram as Figure 2.4. It can be seen that the PVT sim matches the measured data very well. The bubble point pressure and onset asphaltene precipitation pressure data for the reservoir oil A and injection gas mixtures in the swelling are summarized in Table 2.5.

Table 2.5 Bubble point & asphaltene analysis with gas injection

Molar concentration of injection gas	Onset of Asphaltene Precipitation Pressure	Bubble Point Pressure
Mol %	Kpa	Kpa
15	21545	14477
45	34470	22750
60	43150	27878

Commercially package PVT sim and HYSYS software were utilized to determine bubble point and onset asphaltene precipitation to the reservoir fluid A at 397 K in concentrations 15 mole%, 45 mole% and 60 mole% . The bubble point pressure and the onset asphaltene precipitation pressure were obtained and presented on Figure 2.4. The measured onset asphaltene precipitation points were also present in Figure 2.4 . The matching is very good.

The purpose of this work is to determine the domain for asphaltene precipitation.

The obtained results were satisfied so that, it build up our trust to continue the same procedure for fluid oil B.

3.1 The Asphaltene Precipitation By Refractive Index (RI).

Determining refractive index:

In this work for oil B there are two methods to determine asphaltene precipitation, The measured value of RI of 1.4 as suggested by reference

(8), is made to determine the onset pressure of asphaltene precipitation for oil B.

The molecular refraction [R] as reported by James and Prichard was defined as follows:

$$[R]_A = \frac{n_D^2 - 1}{n_D^2 + 1}\frac{M_A}{\rho} \quad ,$$

$$[R]_{A,B} = x_A[R]_A + x_B[R]_B$$

$$[R]_{A,B} = \frac{n_{A,B}^2 - 1}{n_{A,B}^2 + 2}\left(\frac{x_A M_A + x_B M_B}{\rho_{A,B}}\right)$$

HYSYS computer software is used to perform calculations. include the following:

1- Flash calculations of oil & gas mixture to determine the bubble point pressure at the selected reservoir temperature.

2- Refractive index for the single phase fluid is calculated.

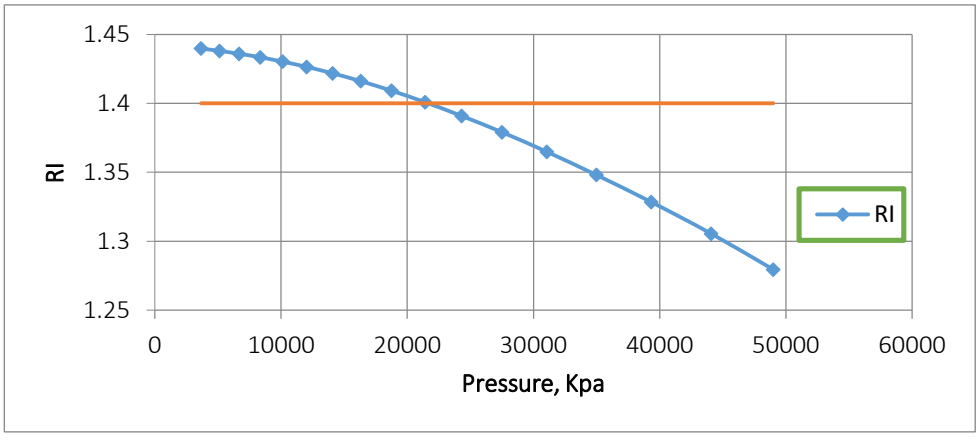

Figure 2.1 showing the pressure with refractive index

The results for oil B & gas mixture in presented on figure 2.1 the results in this method are not as expected. The results obtained by this method failed to determine the asphaltene onset precipitation. Therefore, other techniques are needed to determine the onset asphaltene precipitation region for this oil.

Figure 2.2 presents HYSYS and PVT sim Software predictions of bubble point pressure for oil B and injection gas. The results show very good match.

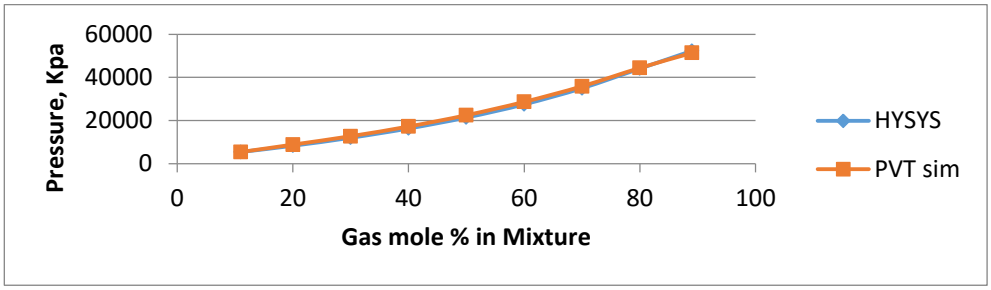

Figure 2.2 : Effect Injection Gas on saturation pressure

3.2 Asphaltene precipitation Determined using PVT sim software

To develop the Asphaltene precipitation envelope for the reservoir oil B, plots of saturation point and upper and lower asphaltene pressure as a function of temperature are presented.

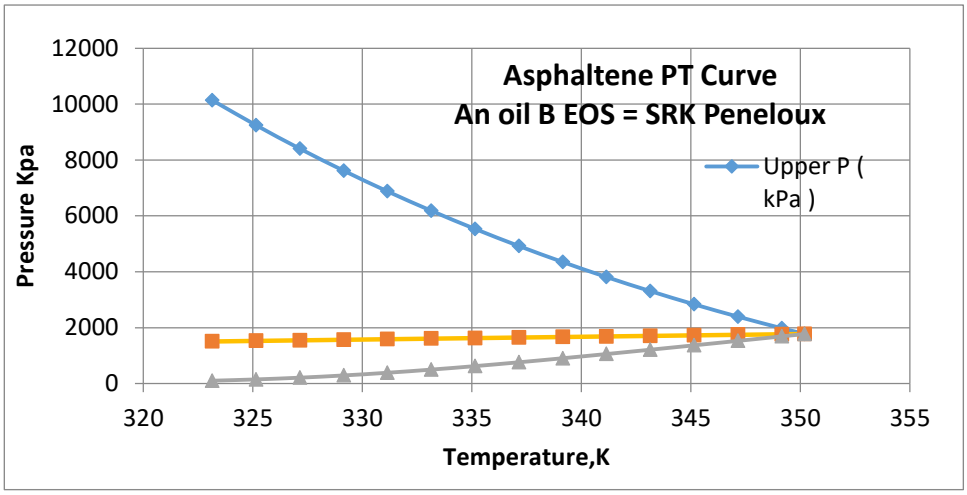

Figure 2.3 Pressures of saturation point, asphaltene precipitation upper and lower asphaltene pressure as function of the temperature for the reservoir fluid B.

According to Figure 2.3, it can be noticed that increase in temperature from 320 to 350 K will result in decrease in upper asphaltene pressure falls by 8360 kPa.

When the temperature is higher than 350 K, the effect of the temperature on the upper asphaltene pressure becomes weak. In comparison to the upper asphaltene pressure, the saturation pressure and lower asphaltene pressure are weakly dependent upon the temperature.

Effect of gas injection on asphaltene precipitation envelope (P–x Curve)

Gas injection is one of the techniques that may be used to maintain or improve recovery. In this work, experimental data from reference[37] for the upper and lower asphaltene onset conditions over a temperature range

from 316-397°K were measured for the reservoir fluid A. In addition, three injection gas mixtures (15, 45, & 60 mole%) were also evaluated at the reservoir temperature of 397°K. This work is reproduced by using PVT sim and HYSYS to confirm its results.

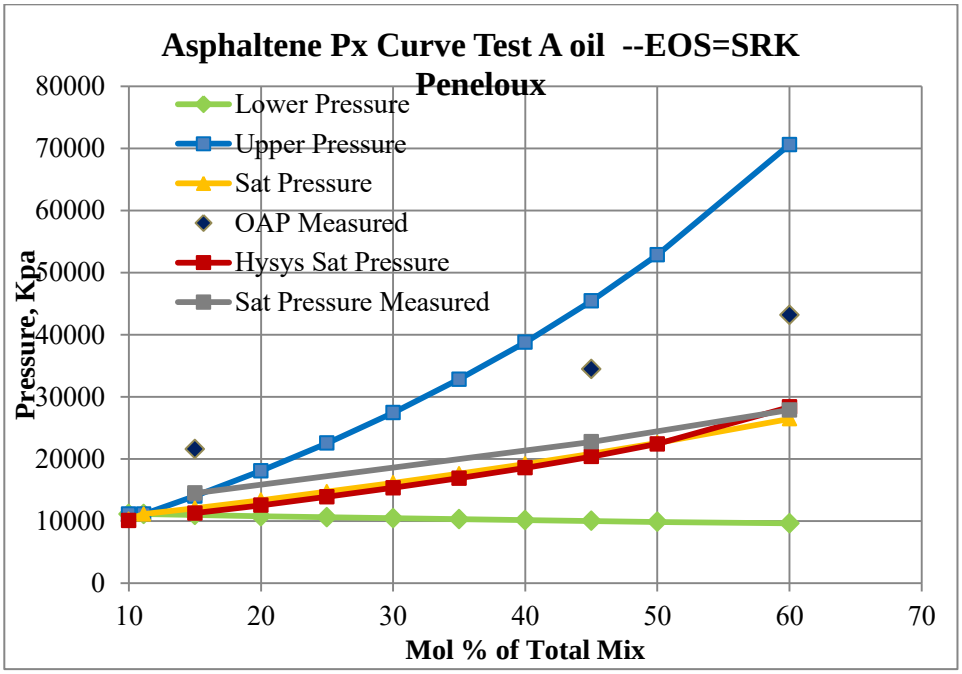

Figure 2.4 Effect of gas injection A on upper asphaltene pressure, bubble (saturation) point pressure and lower asphaltene pressure.

A hydrocarbon gas of known composition is presented in Table 2.4. The injection gas was added to the reservoir fluid at 417 K and 39768 KPa in concentrations 11 mole %, 20 mole%, 30 mole%, 40 mole%, 50 mole%, 60 mole%, 70 mole%, 80 mole% and 89 mole% injection gas, respectively.

However, it is well known that addition of light gases to an asphaltenic oil may result in precipitation of asphaltenes. The gas injection in Reservoir contain the proportion of pure components (N_2, C1, C2, C3, iC4, nC4, iC5, and nC5) and the pseudo-hydrocarbon components (C6, C7) with the composition given in Table 2.4.

The effect of gas mixed with oil B on asphaltene precipitation was investigated at 417 K. As shown in Figure 2.5 gas injection widens the pressure range with asphaltene precipitation.

The (P-x curve) option for reservoir temperature may be used to determine the pressure range with asphaltene precipitation for various amounts of injection gas. It calculates upper asphaltene pressure, bubble (saturation) point pressure and lower asphaltene pressure.

Figure 2.5 Presents the obtained results, injection gas mixtures by using PVT sim the upper asphaltene pressure, bubble (saturation) point and lower asphaltene pressure and also bubble (saturation) point using by HYSYS for the reservoir oil B.

According to the Figure 2.5, increasing the mole percentage of injection gas increases in upper asphaltene precipitation pressure, saturation point pressure and lower asphaltene pressure showing that there is a positive relationship. Asphaltene problems that occurred in reservoir from oil were associated with injection of gas.

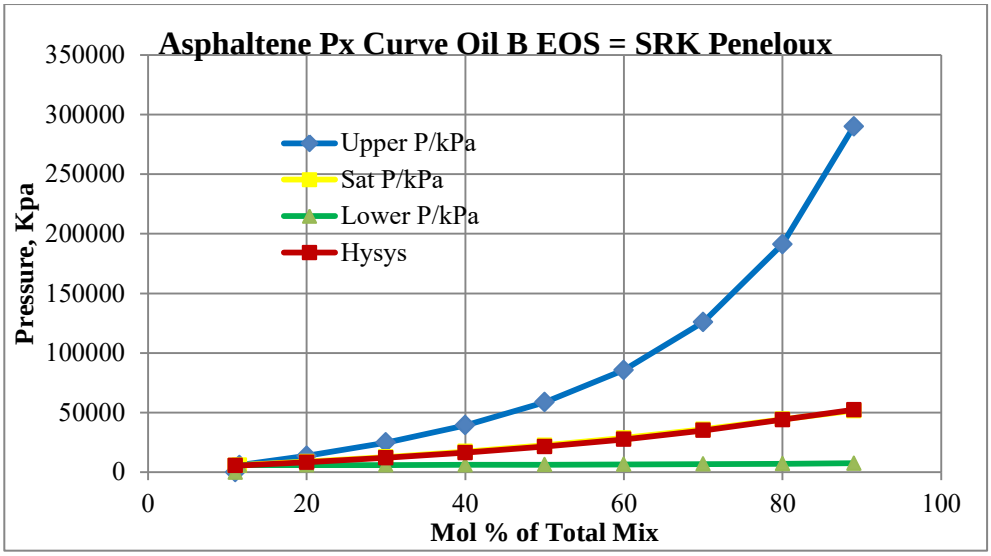

Figure 2.5 Effect of gas injection B on upper asphaltene pressure, bubble (saturation) point pressure and lower asphaltene pressure.

The Asphaltene Precipitation Envelope (APE)

Asphaltene precipitation is likely between the upper and lower asphaltene pressures.

Referring to Figure 2.5, two phases are exist in the region from upper asphaltene pressure to saturation pressure. Also, three phases are exist in the region from saturation pressure to lower asphaltene pressure.

Above the upper asphaltene pressure there is only one liquid phase. Below the lower asphaltene pressure, gas and liquid are present.

4. Conclusions

The onset asphaltene precipitation pressures for two different crude oils were calculated based on the refractive index by HYSYS and PVT sim and compared with experimental work for crude oil A. This work gives confirm

and trust for crude oil B. The onset asphaltene precipitation and bubble point pressure were calculated for each oil with natural gas as injection fluid.

Results show good agreement between calculated and measured data (only for one oil, A). Figures 2.4 and 2.5 for oils A and B present saturation pressure and onset asphaltene precipitation.

References

1. Christensen, J.R., Stenby, E.H. and Skauge, A "Review of WAG Field Experience", SPE 39883, SPE International Petroleum Conference and Exhibition of Mexico, Vilahemosa, Mexico 3-5 March 1998.
2. Christensen, J.R., Stenby, E.H and Skauge, A. 2001. Review of WAG Field Experience. SPE 71203. April 2001, page 97-106.
3. De Boer, R.B, & Leeriooyer K.: "Screening of Crude Oils for Asphalt Precipitation: Theory, Practice, and Selection of Inhibitors," paper SPE 24987 presented at the European Petroleum Conference held in Cannes, France, 16-18 November 1992.
4. Catalan, L.L., Jamaluddin, A.K.M., Stephanic, D.W., McNichol, P.A.: "Solids Problem at the Ring Border Gas Plant," JCPT, 37 (12), December 1998, 48.
5. Koch, H.A. Jr.: "High Pressure Gas Injection Is A Success," World Oil, 143, (Oct 1956), 260.
6. Thomas,. F.B.: "Proposed Screening Criteria for Gas Injection Evaluation," *JCPT*, 37 (11), (November 1998), 14.

7. Burke, N.E., Hobbs, R.E., and Kashou, S.F.: "Measurement and Modeling of Asphaltene Precipitation," *JPT* (November 1990), 1440.

8. Anticipating Asphaltene Problems Offshore—A Practical Approach, J.X. Wang and J.S. Buckley, PRRC, New Mexico Tech, N.A. Burke and J.L. Creek, Chevron Texaco, This paper was prepared for presentation at the 2003 Offshore Technology Conference held in Houston, Texas, U.S.A., 5–8 May 2003.

9. Leontaritis, K.J. and Mansoori, G.A.: "Asphaltene Deposition: A Survey of Field Experiences and Research Approaches," *J. Pet. Sci. Eng.* **1** (1988) 229.

10. A.K.M. Jamaluddin, J.N. Nighswander: Oilphase - A Schlumberger Company Bruce F. Kohse : Computer Modelling Group, Ltd. Ahmed El Mahdi, M. A. Binbrek & P. F. Hogg:. " Experimental and Theoretical Assessment of the Asphaltene Precipitation Characteristics Under a Proposed Miscible Gas Injection Scheme," ADSPE – 0923. Abu Dhabi International Petroleum Exhibition and Conference held in Abu Dhabi, U.A.E., 15–18 October 2000.

11. A.Y. Zekri, Ibrahim El-Agile, Agip Oil., Libya, E Causin, Agip S.P.a.:"Study of a Possible Miscible Flood in Bu Attifel Field," SPE 49521 Abu Dhabi, U.A.E., 11–14 October 1998.

Journal of Total Science
Volume (6), Issue (24) (June. 2023)
ISSN: 2518-5799

مجلة العلوم الشاملة
المجلد (6)، العدد (24)، (يونيو2023)
ردمد: 2518-5799

"AN EXPLORATION ON SELECTED VARIABLES AS A PREDICTORTO COVID-19 VACCINATION ROLLOUTS: A CORRELATIONAL STUDY"

Thabet Al-hani Mohamed Nagah **AttallahGhareba**

Faculty Of Science and Medical Technology, Attahadi University Tripoli, Libya

ABSTRACT:

The study aimed to determine the variables that would predict the vaccination rollouts.

The objective of this study was to determine the acceptance of a coronavirus disease 2019 (COVID-19) vaccine among the general adult population in Libya and assess its determinants. Specifically, it aims to answer the following questions: 1.) What are the variables that would predict the vaccination rollouts, in terms of: a. Knowledge about the vaccine b. exposure to corona virus 2.) What are the respondents level of acceptance to COVID-19 vaccination? 3.) Is there a significant relationship between the predictors of vaccination turnouts and the level of acceptance COVID-19 vaccination? 4The findings that the researcher was able to extract from the study were: 1) the frequency and percentage of the Knowledge as predictor of vaccination turnouts is 94.1% for YES and 5.8% for NO. In terms of exposure to Corona Virus, those who was tested POSITIVE for COVID-19 yielded a result of 29.4% and those tested negative with 70.5%. 2.) Detailed analysis of the results reveals that the level of acceptance of respondents to COVID-19 vaccination is 52.9% for YES they will avail and 47% for NO they wouldn't want to avail. 3.) Both determinants, the knowledge and exposure to corona virus yielded a positive strong relationship with the level of acceptance to COVID-19 vaccination.

KEY WORDS:

- COVID-19, Determinants, Vaccination.

INTRODUCTION:

COVID-19 started from Wuhan city China and has currently afflicted almost the entire world. Coronavirus was also identified back in the years of 2003 and 2015 named as Severe Acute Respiratory Syndrome-Coronavirus (SARS-Cov) and Middle East Respiratory Syndrome-Coronavirus (MERS-Cov), which were similar to COVID-19 and these exhibited similarities to COVID-19 was first reported at the end of December 2019. (1)

Since many cases of the novel coronavirus disease 2019 (COVID-19) first appeared in Wuhan, China, in December 2019, the virus has infected millions worldwide. On January 30, 2020, the World Health Organization (WHO) declared that the outbreak of COVD-19 constituted a Public Health Emergency of International Concern (PHEIC), calling for countries to take urgent and aggressive action against the spread of the virus. (2)

Coronavirus disease (COVID-19) is an infectious disease caused by the SARS-CoV-2 virus. Most people infected with the virus will experience mild to moderate respiratory illness and recover without requiring special treatment. However, some will become seriously ill and require medical attention. Older people and those with underlying medical conditions like cardiovascular disease, diabetes, chronic respiratory disease, or cancer are more likely to develop serious illness. Anyone can get sick with COVID-19 and become seriously ill or die at any age. The best way to prevent and slow down transmission is to be well informed about the disease and how the virus spreads. Protect yourself and others from infection by staying at least 1 meter apart from others, wearing a properly fitted mask, and

washing your hands or using an alcohol-based rub frequently. Get vaccinated when it's your turn and follow local guidance. (3)

Equitable access to safe and effective vaccines is critical to ending the COVID-19 pandemic, so it is hugely encouraging to see so many vaccines proving and going into development. WHO is working tirelessly with partners to develop, manufacture and deploy safe and effective vaccines. Safe and effective vaccines are a game-changing tool: but for the foreseeable future we must continue wearing masks, cleaning our hands, ensuring good ventilation indoors, physically distancing and avoiding crowds. Being vaccinated does not mean that we can throw caution to the wind and put ourselves and others at risk, particularly because research is still ongoing into how much vaccines protect not only against disease but also against infection and transmission. But it's not vaccines that will stop the pandemic, it's vaccination. We must ensure fair and equitable access to vaccines, and ensure every country receives them and can roll them out to protect their people, starting with the most vulnerable. (4)

Vaccines contain weakened or inactive parts of a particular organism (antigen) that triggers an immune response within the body. Newer vaccines contain the blueprint for producing antigens rather than the antigen itself. Regardless of whether the vaccine is made up of the antigen itself or the blueprint so that the body will produce the antigen, this weakened version will not cause the disease in the person receiving the vaccine, but it will prompt their immune system to respond much as it would have on its first reaction to the actual pathogen. Vaccinating not only protects yourself, but also protects those in the community who are unable to be vaccinated. If you are able to, get vaccinated. (5)

Vaccines are a critical tool in the battle against COVID-19, and getting vaccinated is one of the best ways to protect yourself and others from COVID-19. Vaccines train our immune system to recognize the targeted virus and create antibodies to fight off the disease without

getting the disease itself. After vaccination, the body is ready to fight the virus if it is later exposed to it, thereby preventing illness. Most people who are infected with SARS-CoV-2, the virus that causes COVID-19, develop an immune response within the first few weeks. but we are still learning how strong and lasting that immune response is, and how it varies between different people. People who have already been infected with SARS-CoV-2 should still get vaccinated unless told otherwise by their health care provider. Even if you've had a previous infection, the vaccine acts as a booster that strengthens the immune response. There have also been some instances of people infected with SARS-CoV-2 a second time, which makes getting vaccinated even more important. (6)

COVID-19 vaccines are crucial tools in the pandemic response and protect against severe disease and death. Vaccines provide at least some protection from infection and transmission, but not as much as the protection they provide against serious illness and death. More evidence is needed to determine exactly how well they stop infection and transmission.

After being vaccinated, individuals should continue taking simple precautions, such as physical distancing, wearing a mask, keeping rooms well ventilated, avoiding crowds, cleaning hands, and coughing into a bent elbow or tissue. Get tested if you are sick. even if you've been vaccinated.(7)

Vaccines have been a key strategy for improving health outcomes and life expectancy by controlling and preventing infectious diseases, such as smallpox, polio, and plague. Given the elevated morbidity and mortality associated with COVID-19, the development of a safe and effective COVID-19 vaccine is a critical step to halt the pandemic. As of December 23, 2020, there were 61 COVID-19 vaccine candidates awaiting clinical evaluation and 172 candidate vaccines in preclinical evaluation. Nevertheless, misinformation and conspiracy theories surrounding COVID-19 vaccines can highly influence vaccine uptake once available.

Hence. to better understand and inform the public health authorities, the current study sought to assess the acceptance of a potential COVID-19 vaccine and evaluate factors that influence its acceptance among the adult population in Tripoli, Libya. (8)

The COVID-19 pandemic continues to impose enormous burdens on morbidity and mortality while severely disrupting societies and economies worldwide. Governments prepare themselves to ensure large-scale, equitable access and distribution of safe and effective COVID-19 vaccines. Overcoming the pandemic will require sufficient health system capacity, and effective strategies to enhance trust in and acceptance of vaccines. Concern about vaccine hesitancy is growing worldwide. For decades, vaccines have been a successful measure to eliminate and prevent numerous infections. However, vaccine hesitancy and misinformation act as hurdles in achieving high coverage and community immunity against the infection. In 2015, the World Health Organization (WHO) Strategic Advisory Group of Experts on Immunization stated vaccine hesitancy as a "delay in acceptance or refusal of vaccination

despite the availability of vaccination services". Vaccine hesitancy can differ in form and intensity based on when and where it occurs and what vaccine is involved.

Concerns about vaccine hesitancy are growing globally, prompting the World Health Organization (WHO) to declare it among the top ten health threats in 2019.

Governments, public health officials, and advocacy groups must be equipped to address vaccine hesitancy. There is a need to build vaccine literacy to increase vaccine acceptance rates. Besides, misinformation spread through multiple sources could have a considerable impact on the acceptance of a COVID-19 vaccine. Governments and societies must gauge current levels of willingness to receive potentially safe and effective COVID- 19 vaccines and identify correlates of vaccine hesitancy and/or acceptance. Intervention models to improve vaccine literacy and acceptance should directly take up community-specific concerns, misconceptions, and be sensitive to religious or cultural beliefs. Researchers have recognized effective interventions for building confidence and decreasing vaccine hesitancy in different contexts. Trust in government is highly associated with vaccine acceptance and can contribute to public compliance with recommended actions. Addressing and overcoming vaccine hesitancy requires more than building trust. Clear and consistent effective communication by government officials is central in building public confidence in vaccine programs. This includes explaining how vaccines work, their development, along regulatory approval based on safety and efficacy. Powerful campaigns should also aim to explain the effectiveness of vaccines, the time needed for protection, and the

significance of population-wide vaccine coverage to attain community immunity. Inculcating public confidence in regulatory agency reviews of vaccine safety and effectiveness will be imperative. Despite tremendous efforts being made to achieve COVID-19 vaccine coverage, vaccine hesitancy could be a major barrier toward its acceptance by the general population. To identify the scope of the problem, the current scoping review aims to explore and understand the rates of acceptance and hesitancy related to COVID-19 vaccine among the population globally. This could help bridge the knowledge gaps and facilitate formation of effective strategies to overcome the high levels of hesitancy related to COVID-19 vaccine, increase its uptake, and mitigate the pandemic as well as help global stakeholders to conduct COVID-19 vaccination drives and promote vaccine uptake.

At this juncture, we bent on the study entitled "An Exploration on selected Variables as a Predictor to COVID-19 Vaccination Rollouts: A Correlational Study."

METHODS:

This study employed the Descriptive Correlational method of research. The respondents of this study were the guests of Attahadi University during the World Oral Health Day where they had their COVID-19 testing done. While participating in the event, some guests were asked of the data needed for the variable of knowledge and their perception as to would they avail the vaccine for COVID-19 or not. The other predictor variable which is their exposure to corona virus was determined through the result of their

Rapid PC test. The convenience or accidental sampling was utilized in this study.

The researcher made use both of primary data and secondary data as well as a tool in collecting data. The questionnaire was used for the variables of knowledge and the acceptance of vaccination program while the exposure to corona virus is through secondary data. After the data was retrieved, it was treated statistically.

RESULTS:

Detailed analysis of Figure 1-A showing the frequency and percentage of the Knowledge as predictor of vaccination turnouts is 94.1% for YES and 5.8% for NO.

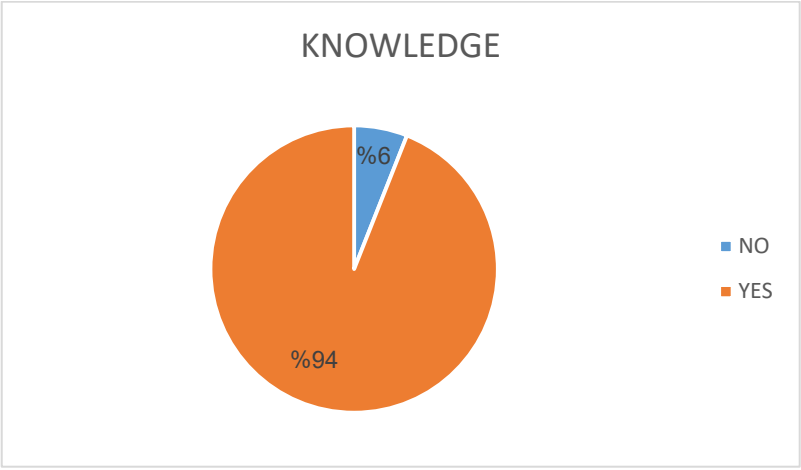

FIGURE 1-A

Cursory inspection of Figure 1-B reflecting the results of frequency & percentage of exposure to Corona Virus, those who was tested POSITIVE for COVID-19 yielded a result of 29.4% and those tested negative with 70.5%.

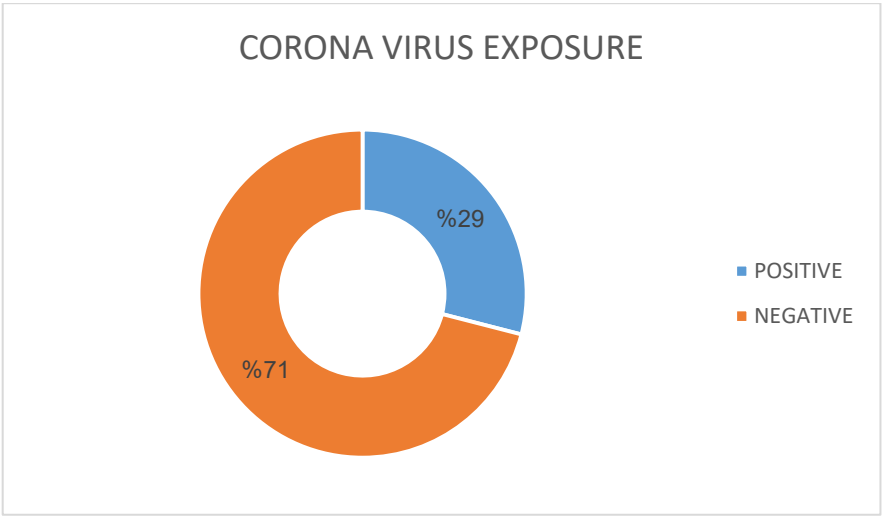

FIGURE 1-B

Figure 2 of the level of acceptance of respondents to COVID-19 vaccination reveals that 52.9% YES they will avail and 47% for NO they wouldn't want to avail.

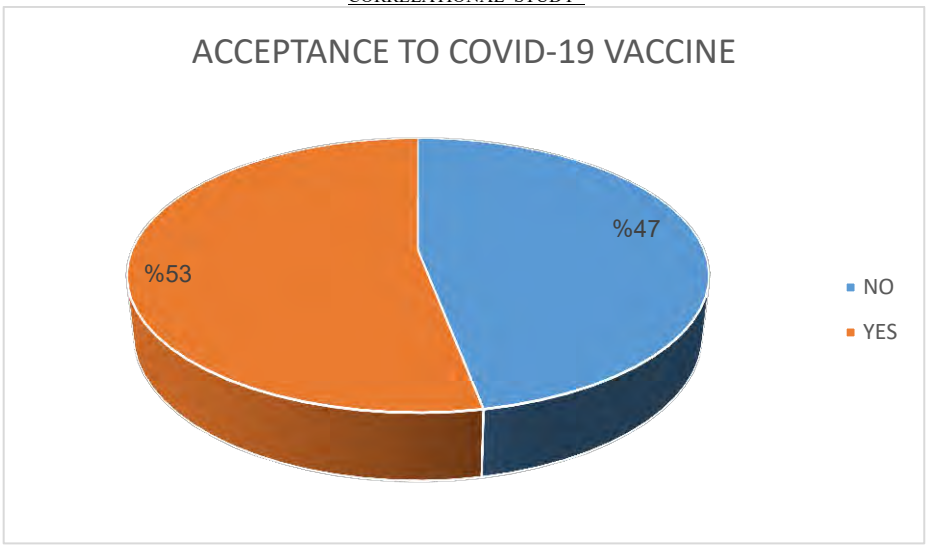

FIGURE 2

Detailed analysis of Figure 2 reflecting the results of the frequency and percentage of the level of acceptance to COVID-19 vaccination. Though the results show a higher percentage on the response of "YES" which is 53%, it is still worthwhile to note that there is a significant value of 47% that responded "NO".

Pearson Momentum Correlation between the Knowledge of the Respondents on COVID – 19 and the Acceptance of COVID-19 Vaccine.

Variables		
Knowledge	Pearson Correlation	0.78
(X)	Level of Sig	.349
	N	34
Academic Performance	Pearson Correlation	0.78
in Major Nursing Subjects	Level of Sig	.349
(Y)	N	34

There was a positive strong correlation between the two variables, r=0.78 n=34, p=.349

Pearson Momentum Correlation between the Exposure of the Respondents on COVID – 19 and the Acceptance of COVID-19 Vaccine.

Variables		
Exposure to COVID-19	Pearson Correlation	0.89
(X)	Level of Sig	.349
	N	34
Academic Performance	Pearson Correlation	0.89
in Major Nursing Subjects	Level of Sig	.349
(Y)	N	34

There was a positive strong correlation between the two variables, r=0.89 n=34, p=.349

DISCUSSION:

For statement of the problem #1-A, particularly on knowledge as determinant to the COVID - 19 vaccination, a high percentage result of 94% reveals an adequate knowledge among the participants. This is the same with the other studies conducted. Most of the participants had adequate knowledge related to COVID- 19. Despite adequate knowledge, the attitude was not always positive, thereby necessitating further education to convey the importance of forming a positive attitude and continuous preventive practice towards reducing contraction and transmission of COVID-19. (9)

Findings demonstrated that the respondents have adequate knowledge about COVID-19, including the transmission of the virus through respiratory droplets of infected people and clinical symptoms of the disease. The perceived risk for infection susceptibility was relatively lower than the disease's perceived severity regarding attitudes. The impact of efficacy beliefs on preventive measures was high in both personal hygiene and social distancing. Most respondents complied with the recommended practices such as wearing facial masks, practicing hand hygiene, and social distancing to prevent COVID- 19 infections.(10)

To decrease the adverse effects of COVID-19, there is a need to increase the general public's knowledge so that spread of the disease can be reduced. Poor understanding of COVID-19 in the general public can result in delayed identification and can be a key factor in the rapid spread of disease. (11)

Statement of the problem #1-B, on the exposure to corona virus, shows that most of respondents were tested positive for the corona virus which yielded a result of 71%. The first case of COVID-19 was identified in Libya on 24/3/2020, and about 2 months later, the number of reported COVID- 19 cases started to increase notably. The outbreak was first prominent in the southern region (Sabha) and then spread to the western and eastern parts of Libya. By 24/12/2020, the reported total number of deaths from COVID-19 reached 1415. There seems to be no published data on the size of the epidemic in Libya. Here, we estimated the number of Libyans exposed to COVID-19 by using a COVID-19 mortality adjusted mathematical model for the spread of infectious diseases. We estimated that 14-20% of the Libyan population have been exposed to the COVID-19 pandemic. Thus, the risk of spread of COVID-19 infections during the coming months is high, and a considerable number of Libyans, particularly the elderly and people with chronic diseases, should be protected against COVID-19 infection. This is particularly urgent in the light of unofficial reports that the relevant healthcare facilities are under extreme stress. (12)

Libya is witnessing an alarming surge in COVID-19 cases in the last 2 weeks where infections area at their peak. The National Centre for Disease Control (NCDC) recorded4,061 new COVID cases on the 18th of July, the highest daily rate since the onset of the pandemic.

Libya has surpassed 221.495 new COVID- 19 cases since the beginning of the pandemic as the highly contagious Delta variant persists in the neighboring countries and most likely is in Libya. The virus is rapidly spreading across Libya with a 270% increase in COVID-19 cases in the West, 480% in the South and 50% in the East of the country. These

numbers are terrifying enough but the actual number of cases is likely to be much higher due to acute shortages of tests and laboratory capacity.

"We are alarmed at the rapid spread of the virus in the country," said AbdulKadirMusse, UNICEF Special Representative in Libya. "The vaccination rate is very low, and the spread is fast. We must be faster in our response. The most important thing we can do to stop the spread of COVID-19, and the variants, is ensure everyone who is eligible gets vaccinated. Countries with high coverage of two doses of vaccines have been able to drastically reduced rate of hospitalization and deaths. We also need follow and abide to preventive measures.", he added. Already disrupted by years of instability, the Libyan healthcare system is further challenged with high rates of community transmission and is struggling to curb the rapid spread and to meet the population's needs. (13)

Statement of the problem #2 reveals an increase in the acceptance of COVID - 19 vaccine among the respondents. However, despite the increase in percentage of 53%, the remaining 47% of the pie is worth taking note of. A range of organizations within and beyond the health sector can play a vital role in sharing accurate information about vaccination and its benefits. Almost everyone can play their part by knowing the basics of vaccination and the reliable sources for more details, as well as by openly expressing their enthusiasm for getting vaccinated. Organizations and employers can boost confidence by openly sharing their support for vaccination, or personal experience of getting vaccinated. This helps to promote vaccination acceptance as a social norm in the workplace. One of the best ways to address people's concerns about getting vaccinated is to refer them to someone they trust. Remember that

these concerns can be emotional for people and touch on issues outside of science, such as their personal experiences and their perceptions of poor or unfair treatment in the past. Don't overwhelm people with facts and information. Instead. acknowledge their perspectives or experiences and speak to their motivations, not what you think they need to hear. Vaccination will help keep you, your family and your community safe from COVID-19,and will bring usallclosertodoingthethingswelovewiththepeoplewecareabout[14]

Hence, vaccine hesitancy, described as a "delay in acceptance or refusal of vaccination despite availability of vaccination services", can hamper future COVID-19 vaccination efforts. Currently, little is known about the acceptance of a potential COVID-19 vaccine and factors that influence its acceptance, although such information is essential in planning strategies to increase vaccine acceptability before a vaccine becomes available.

In this study, we found that 53.1% of the total study participants demonstrated willingness to receive vaccination against COVID-|9 once a vaccine is available. Such a level of acceptability is considerably low given the magnitude of the COVID-19 pandemic. Prior estimates suggest that the threshold for COVID- 19 herd immunity varies among countries, with a suggested average threshold of approximately 67%. Hence, the observed acceptance level of 53.1% in the current report indicates an urgent need for public health strategies to increase acceptance of potential COVID- 19 vaccines in the general population.

In total, only 53.1% of our study participants were willing to receive vaccination against COVID-19 once a vaccine becomes available, with several factors influencing the level of acceptance. Such findings are of public health importance and should guide public health efforts in increasing acceptance of vaccination against COVID-19 in the population at large. Although an effective and safe vaccine against COVID- 19 is a key element in controlling and bringing an end to the COVID-19 pandemic, ensuring wide acceptability of the vaccine is essential. Hence, public health strategies are urgently needed to address the wide misinformation and conspiracy theories surrounding COVID-19 vaccines. Moreover, transparent communication about vaccine effectiveness and safety will contribute to increasing public trust in future COVID-19 vaccination programs. (15)

Statement of the Problem #3, reveals that both variables of knowledge and exposure to corona virus have a significant positive strong relationship with the level of acceptance to COVID-19 vaccination. During health crises and emergencies, the public needs to practice precautionary behaviors at all times, as the novelty and unpredictability of epidemics may exceed a health system's capability to a significant degree. This study provides evidence that knowledge is an essential predictor of attitudes and behaviors, contributing to advancing intervention strategies to promote and sustain the public's precautionary behaviors in the context of the COVID-19 pandemic. (16)

To increase precautionary behaviors among the public, health officials and policymakers must promote knowledge and efficacy belief. Future interventions and policies should also be developed in a 'person-centered? approach, targeting vulnerable subgroups, embracing them, and closing the gap of KAP toward COVID- 19. (17)

Participants who considered vaccination important for their own health or for the health of the community were more willing to accept vaccination. This suggests that if more people are educated about the importance of vaccination against COVID-19, their willingness to be vaccinated will increase. (18)

Therefore, the knowledge, attitude, and practices people possess regarding COVID-19 play a key role in determining a society's readiness to accept behavioral change measures from the health authorities.

Measurement of the public's knowledge, attitudes, and practices will help provide a better understanding of the COVID- 19 and the establishment of health-promoting advertisement and preventive strategies. (19)

In multivariable analysis, subjects above 60 years and healthcare workers were more likely to accept the SARS-CoV-2 vaccine. Irrespective of the COVID test result, participants who had previously been tested for COVID- 19 were more willing to take the vaccine compared to those who were never tested. Moreover, participants who were "extremely concerned" about COVID-19 (re)infection and those who suffered from a chronic disease had higher odds of accepting the SARS-CoV-2 vaccine. Finally, participants who Vaccines 2021, 9, 828 5 of 10 considered vaccination

important for their own health or for the health of the community were more willing to accept vaccination, compared to those who considered vaccination not or less important.

Globally, the average rate of vaccine hesitancy in April 2020 was 21%, which increased to 36% in July 2020 and later declined to 16% in October 2020. Large variability in vaccine acceptance and high vaccine hesitancy can influence the efforts to eliminate the COVID-19. Addressing the barriers and facilitators of vaccines will be crucial in implementing effective and tailored interventions to attain maximum vaccine coverage.[20]

CONCLUSIONS:

It can be said that most of the respondents are knowledgeable on COVID - 19 and that among the respondents who were tested for COVID-19 yielded a negative result. Both determinants were proved to be predictors in the level of acceptance to COVID-19 vaccination. Therefore, the results of this study can be considered as baseline data in the policy making procedures of the health sector in its efforts of providing programs in addressing the effects of pandemic in the Libyan populace.

REFERENCES:

1 - https://journals.sagepub.com/doi/full/10.1177/0272684X211004945

2 - https://bmcpublichealth.biomedcentral.com/articles/10.1186/s12889-021-10285-y

3 - https://www.who.int/health-topics/coronavirus#tab=tab-1

4 - https://www.who.int/emergencies/diseases/novel-coronavirus-2019/covid-19-vaccines

5 - https://www.who.int/news-room/feature-stories/detail/how-do-vaccines-work

6 - https://www.who.int/news-room/feature-stories/detail/getting-the-covid-19-vaccine

7 - https://www.who.int/news-room/feature-stories/detail/vaccine-efficacy-effectiveness-and-protection

8 - https://www.karger.com/Article/FullText/514636

9 - https://journals.plos.org/plosone/article?id=10.1371/journal.pone.0249853

10 - https://journals.sagepub.com/doi/full/10.1177/0272684X211004945

11 - https://bmcpublichealth.biomedcentral.com/articles/10.1186/12889-021-10285y

12- https://www.tandfonline.com/doi/full/10.1080/19932820.2021.1871798

13-https://reliefweb.int/report/libya/unicef-alarmed-surge-covid-19-cases-amid-low-vaccination-rates-libya-enar

14 - https://www.who.int/news-room/feature-stories/detail/how-to-talk-about-vaccines

15 - https://www.karger.com/Article/FullText/514636

16- https://bmcpublichealth.biomedcentral.com/articles/10.1186/s12889-021-10285-y

17 - https://bmcpublichealth.biomedcentral.com/articles/10.1186/12889-021-10285-y

18 - https://www.mdpi.com

19 - https://journals.sagepub.com/doi/full/10.1177/0272684X211004945

20 - https://www.frontiersin.org/articles/10.3389/fpubh.2021.698111/full

Journal of Total Science
Volume (6), Issue (24) (June. 2023)
ISSN: 2518-5799

مجلة العلوم الشاملة
المجلد (6)، العدد (24)، (يونيو2023)
ردمد: 2518-5799

Crowding in and Crowding out Hypothesis

Case Study of Libya (1962-2007)

Rasheed Muftah Salem

Associate Professor

Department of Economics, Faculty of Economics and Political Science,

University of Tripoli

Abstract

The study aims to explore the Crowding in and Crowding out Hypothesis in the Libya's economy from 1962 to 2007 employing the VAR technique as the appropriate method to answering the question of whether public investment crowds out private investment or not. The results revealed that, though the coefficient of public investment is insignificant, the negative sign appears to suggest that public investment crowds out private investment, and that public investment has no a favourable impact on private investment. This may raise some concern in terms of political intervention throughout the economy and the hostility which discouraged the private investment environment. The study suggests that private and public investment should be formulating complementary relationship, and that it may be advisable for the government to privatize firms in the economy so as to induce the inflow of private investment.

الملخص

تهدف هذه الدراسة لمعرفة فرضية المساندة والمزاحمة بالإقتصاد الليبي خلال الفترة من عام 1962 إلى عام 2007 وذلك بتوظيف نموذج الإنحدار الذاتي كطريقة مناسبة للإجابة عن السؤال ماإذاالإستثمار العام مزاحم للإستثمار الخاص أم لا. فقد أظهرت النتائج وبرغم عدم معنوية معامل الإستثمار العام، فإن العلامة السالبة تظهر بأن الإستثمار العام يزاحم الإستثمار الخاص. ربما هذا يوجه النظر فيما يتعلق بالتدخلات السياسية بالإقتصاد والنفور الذي يحبط بيئة عمل القطاع الخاص. لذلك تقترح الدراسة بأن ينبغي تشكيل علاقة مكملة بين القطاع الخاص والعام، وأنه من الأفضل بالنسبة للحكومة أن تعمل لتخصيص المنشات العامة وذلك لتشجيع تدفق القطاع الحاص بالإقتصاد.

1. Introduction

The crowding out emphasizes that public investment will adversely impact private investment through uncompetitive business environment. On contrary, the crowding in exhibits that public investment will positively impact private investment. The link betweenpublic and private investment concentrates on whether public investment services private investment. But more crucially, enhancing more attention has recently been paid to the crowding in and crowding out hypothesis. Public and private investment has a vital role to economic growth. Therefore, examining the relationship between public and private investment gives an indicator to answering the question of whether public investment crowds out private investment or not.

2. Literature Review

To shed light on this issue, this study aims to empirically carry out the crowding in and crowding out hypothesis by conducting the VAR approach to test the relationship among private investment, public investment and gross domestic product.Differentpoints of view presented in the literature review.Agenor et al. (2005)[1] tested the impact of public capital on private capital in Egypt, Jordan and Tunisia from 1965 to 2002 using VAR approach. They found that there is a week insignificant impact of public capital on private capital. Ejaz and Musleh (2006)[2]analyzed the impact of public investment on economic growth in the contest of Pakistan's economy using VAR technique for the period from 1973 to 2004. They

[1]. (Agenor and et al, Public Infrastructure and Private Investment in the Middle East and North Africa, 2005). https://opennowledge.worldbank.org.
[2]. (Ejaz, and Musleh, 2006, p.94).

revealed that public investment crowds out private investment, and that public investment has a negative though insignificant impact on economic growth. Belloc and Vetova (2006)[3] conducted a study to test the relationship between public investment and output in seven highly indebted countries from 1970 to 1991 employing VECM method. They showed that in six of the seven cases there a positive effect of public investment on output.Xiaoming and Yanyang (2014)[4] examined the nexus between public investment and private investment in China using VAR method for the period $1980-2011$. They revealed that public investment in public commodities crowd in private investment, and that public investment in private commodities crowd out private investment.Gbenga, et al (2020)[5] examined the relationship between public investment and private investment in Nigeria utilizing VAR technique for the period $1980-2016$. They found that public investment on physical assets crowd out private investment, and that public investment on human investment crowd out private investment.

3. Data and methodology

The study uses the VAR approach to examine the crowding in and crowding out hypothesis.

The VAR consists of three variables, private investment (IP), public investment (IG), and output (GDP). Data on these variables are collected from Economic Research Center of Benghazi for the period $1962-2007$. The disaggregation of investment into public and private components not

[3]. (Belloc and Vertova, 2006, p.151).
[4]. Xiaoming and Yanyang, 2014, p.1).
[5]. (Gbenga, 2020, p.71).

only allows the question of whether or not public investment crowds out private investment, but, in addition to this, sheds light on the impact of the two types of investment on output on the long-run co-integration relationship. Thus, to avoid the potential problem of estimating spurious relationships, the time series properties of the variable under investigation are tested for unit roots.

4. Test results for unit roots results

To avoid the potential problem of estimating spurious relationships, it is necessary to test the time series properties of the variable under investigation.

Each time series in our simple of $lnGDP$, $lnIP$, and $lnIG$ are first tested for their order of integration by using Augumented Dicky-Fuller (ADF) test.

We use an Augumented Dicky-Fuller test to help determine whether the process has a unit root. They actually consider three different equations that can be used to test the existence of a unit root.

$$Dy_{t=c_0} + \gamma y_{t-1} + c_2 t + \varepsilon_t \qquad (1)$$

$$Dy_{t=c_0} + \gamma y_{t-1} + \varepsilon_t \quad (2)$$

$$Dy_{t=} \gamma y_{t-1} + \varepsilon_t \ (3)$$

The difference between the three equations concerns the existence of intercept and time trend. The first includes both intercept and linear time trend. If we inappropriately omit time trend, the power of the test can go to zero.

The following hypothesis were formulated and tested to examine whether the process has a unit root. We use a 5% level significance.

H_0 : There is a unit root, which means that the series is non stationary.

H_1 : There is no a unit root, which means that the series is stationary.

$lnGDP$,$lnIP$, and $lnIG$ were tested for their orders of integration by using Augumented Dicky-Fuller (ADF) tests (table 1). Refer to equations (1) , (2) and (3) for the testing equations. The tests showed that $lnGDP$,$lnIP$, and $lnIG$ are integrated of order one.

Table (1) Augumented Dicky-Fuller (ADF) test results for unit root.

Variable	Level	P-value	First difference	P-value
$lnGDP$	Trend and intercept	0.5642	Trend and intercept	0.0029*
	Intercept	.06879	Intercept	0.0004*
	None	0.9655	None	0.0080*
$lnIP$	Trend and intercept	0.0071	Trend and intercept	0.0000*
	Intercept	0.4582	Intercept	0.0000*
	None	0.8660	None	0.0000*
$lnIG$	Trend and intercept	0.3210	Trend and intercept	0.0068
	Intercept	0.2307	Intercept	0.0016
	None	0.9506	None	0.0005

Note:*indicates that variable is integrated of order one because p-value is less than 0.05.

In general, the ADF unit root test suggests that the time series of all variables in (1) to (3) are integrated process of order 1. Since each of these variables are integrated in an order ~ (1), we proceed to the next stage , which determines whether these variables are co-integrated.

5. Test results for co-integration

Since the time series of $lnGDP$, $lnIP$, and $lnIG$ were found to be integrated of the same order

(i.e., order one), a co-integration test could be conducted to deter whether a long-run relation exists among the variables. A Johansen co-integration test is performed, assuming a co-integrating relationship as specified by equation (4).

$$lnGDP_t + a_1 lnIP_t + b_1 lnIP_t + c_1 lnIG_t + A = \varepsilon_{1t} \qquad (4)$$

The Johansen co-integration test can be expressed as follows

H_0: There is no co-integrating relation (r =0).

H_1: There is no co-integrating relation ($r \geq 1$).

Where (r) denotes the number of co-integrating vectors.

Table (2) reports the results of the Johansen test. The test outcome indicates that the maximum Eigenvalues and Trace statistics strongly reject the null hypothesis of no co-integration in favour at least one co-integrating relationship, and that linear trend assumption (intercept no trend) is selected.

Co-integration relationship is found in table (3). In the model there exists a significant long-run relationship in equation (5). However, while there exists a significantly positive relationship between public investment (IG) and output (GDP) , private investment (IP) has an insignificant negative long-run relationship impact on output (GDP).

6. Estimates of the long-run co-integrating equation

A Johansen co-integrating test was performed assuming a co-integrating relationship as specified by equation (4):

$$lnGDP_t + a_1 lnIP_t + b_1 lnIP_t + c_1 lnIG_t + A = \varepsilon_{1t} \qquad (5)$$

We thus proceed to estimate equation (5). The results of long-run co-integrating equation are presented in table (3):

Table (2) Determination the number of co-integrating relations by model GDP, $lnIP$, and $lnIG$.

Date: 02/03/23 Time: 20:30

Sample (adjusted): 1964 2007

Included observations: 44 after adjustments

Trend assumption: Linear deterministic trend

Series: LNGDP LNIP LNIG

Exogenous series: D69 D81 D87

Warning: Critical values assume no exogenous series

Lags interval (in first differences): 1 to 1

Unrestricted Cointegration Rank Test (Trace)

Hypothesized No. of CE(s)	Eigenvalue	Trace Statistic	0.05 Critical Value	Prob.**

None *	0.526241	52.01524	29.79707	0.0000
At most 1 *	0.341656	19.14476	15.49471	0.0134
At most 2	0.016935	0.751536	3.841466	0.3860

Trace test indicates 2 co-integrating eqn(s) at the 0.05 level

* denotes rejection of the hypothesis at the 0.05 level

**MacKinnon-Haug-Michelis (1999) p-values

Co-integration relationship is found in table (3). In the model there exists a significant long-run relationship in equation (5). However, while there exists a significantly positive relationship between public investment (IG) and output (GDP) , private investment (IP) has an insignificant negative long-run relationship impact on output (GDP).

Table (3) The results of long-run co-integrating equation

Vector Error Correction Estimates

Date: 02/03/23 Time: 21:11

Sample (adjusted): 1964 2007

Included observations: 44 after adjustments

Standard errors in ( ) & t-statistics in [ ]

Co-integrating Eq:	CointEq1

LNGDP(−1)	1.000000
LNIP(−1)	0.005092
	(0.05596)
	[0.09099]
LNIG(−1)	−0.789673
	(0.03858)
	[−20.4701]
C	−3.370681

Note:

1. The co−integration coefficients are normalized on the $lnGDP$.
2. T−statistics are in parentheses.
3. The length of the lag is (1) choosing according to VEC lag exclusion Wald test.
4. The model contains D69 (change in the government).
5. The model contains D81 (sharp decline in oil prices).
6. The model contains D87 (steps have been taken towards liberalization).

7. The estimation of vector error-correction model

The next step is the estimation of vector error-correction model, which can be used to ascertain the direction of causation in a multivariate context. The vector error-correction model captures the short run dynamics of the system as well as adjustment towards long-run equilibrium.

As can be seen from table (4) , the error correction term has the right significant sign on output and private investment. In contrast, the error correction term has the wrong sign on public investment, thus the public investment equation will not be taken into consideration.

The empirical results indicate that output is not driven by public nor private investment. Private and public investment has an adverse though insignificant impact on output. In other word, output is not responsive to public and private investment. This may raises some concern in terms of political intervention throughout the economy and the hostility which discouraged the private investment environment. On the question of whether or not public investment crowds out private investment, the results revealed that, though the coefficient of public investment is insignificant, the negative sign appears to suggest that public investment has no a favourable impact on private investment.

Table (4) reports the vector error-correction model

Error Correction:	D(LNGDP)	D(LNIP)	D(LNIG)
CointEq1	−0.328990	−1.220444	0.613264
	(0.11073)	(0.77383)	(0.23689)
	[−2.97121]	[−1.57715]	[2.58882]
D(LNGDP(−1))	0.087056	0.626276	−0.104895
	(0.15427)	(1.07818)	(0.33006)
	[0.56429]	[0.58086]	[−0.31781]
D(LNIP(−1))	−0.028849	−0.491418	0.031831
	(0.02225)	(0.15553)	(0.04761)
	[−1.29632]	[−3.15959]	[0.66855]
D(LNIG(−1))	−0.072442	−0.212046	0.453403
	(0.08658)	(0.60511)	(0.18524)
	[−0.83666]	[−0.35042]	[2.44764]
C	0.231540	−0.098183	0.319019

	(0.06810)	(0.47595)	(0.14570)
	[3.39987]	[−0.20629]	[2.18956]
D69	−0.139384	−0.291069	0.001410
	(0.05985)	(0.41825)	(0.12804)
	[−2.32901]	[−0.69592]	[0.01101]
D81	−0.257584	−0.074385	−0.150613
	(0.06071)	(0.42426)	(0.12988)
	[−4.24313]	[−0.17533]	[−1.15967]
D87	0.164163	0.914237	−0.409054
	(0.07394)	(0.51673)	(0.15818)
	[2.22028]	[1.76927]	[−2.58593]

8. Conclusions

The study assesses empirically the Crowding in and Crowding out Hypothesis. The main conclusions of this study can be summarized as follow:

1. The ADF unit root test suggests that each variable each variable is integrated process of order one, table1.
2. There evidence of long-run relationship between output, private investment, and public investment.
3. Over the long-run, output is insignificantly and negatively related to private investment, and positively to public investment.
4. This is to say, private and public investment is not complementary and private investment would meet a hostile environment.
5. Over the short-run, the error correction term has the right and significant sign on output, and private investment has the right sign but not highly significant. In contrast, the error correction term has the wrong sign on public investment.
6. Output is not driven by public or private investment.
7. This is to say, concerns should be taken into account into the efficiency of public investment and the week role of private investment.
8. Over the short-run, public investment has a negative, but insignificant, impact on private investment.
9. This is to say,public investment crowds out private investment.

References

Agenor,P. and et al. (2005). Public Infrastructure and Private Investment in the Middle East and North Africa, https://opennowledge.worldbank.org.

Belloc, M. andVertova, P. (2006). Public Investment and Economic Performance in Highly Indebted Poor Countries: An Empirical Assessment. *International Review of Applied Economics*, 20(2): 151-170.

Ejaz, G. and Musleh, E (2006). The Impact of Public Investment on Economic Growth in Pakistan. *The Pakistan Review*, 45(1) , 87-98.

Gbenga, et al. (2020). Government Capital Expenditure and Private Sector Investment in Nigeria: Co-integration Regression and Toda Causality Analysis. *Advanced Journal of Social Science*, 6(1): 71-82.

Xiaoming, X. and Yanyang, Y. (2014). Does Government Investment Crowd Out Private Investment in China?.*Journal of Economic Policy Reform*. 18(1): 1-12.

Journal of Total Science
Volume (6), Issue (24) (June. 2023)
ISSN: 2518-5799

مجلة العلوم الشاملة
المجلد (6)، العدد (24)، (يونيو2023)
ردمد: 2518-5799

Performance of Adaptive Power System Stabilizer in Single Machine Infinite Bus

Samah Abdelsalam Dweher

Higher Institute for Technology and Science, Regdalleen,

Libya

Tawfiq H. Elmenfy

Department of Electrical and Electronics Engineering, Faculty of Engineering

University of Benghazi, Libya

Abstract–

This paper proposed adaptive fuzzy controller as a power system stabilizer (AFPSS) used to damp local area modes of oscillation following small and large disturbances in power system. In contrast to the conventional PSS, proposed fuzzy-based stabilizers are more efficient because they cope with oscillations at wide range of operating points. The proposed controller is a fuzzy logic controller based PSS that has the capability to re-tune its fuzzy rule-base on real time. The change in the fuzzy rule base is done using a variable-structure technique to achieve optimum performance. The adaptive algorithm of the proposed controller significantly reduces the rule base two dimensions size due to its adaptively and improves its performance. This statement is confirmed by simulation results of a single machine infinite-bus system under variuos operating points .

Keywords: Fuzzy Logic Control, Adaptive Control, Power system stabilizer and single machine infinite bus

1. Introduction

Power system stability is defined as the ability of the power system to return or remain in its equilibrium point that following small and large disturbances. Power system are becoming increasingly stressed because of growing demand and restrictions on building new power plants and

lines. One of the consequences of such a stressed system is the threat of losing stability following a disturbance due to poor power system stabilizer (PSS) designed. So, the increasing of power transfer capability and improvement power system stability is necessary to enhancement [1].

Power systems are complex due to its hardly nonlinear and unpredictable fault locations, that often have low frequency oscillations due to poor damping caused by wide range of operating conditions which can lead to loss of synchronism and cascade blackout [1]. Conventional or linear Power system stabilizers (CPSS) can provide supplementary feedback control signal to excitation system to damp these oscillations [1–4]. The tune of the fixed parameters of these conventional stabilizers are usually based on the linearized model of the power system around a small range of operating points. Operating conditions change as load variations and wide of power generations. These wide range of operating conditions affect power system dynamic behavior which requires fine-designed and tuned PSS [1–4].

Adaptive controller can re-tune its parameters and structure on-line when the power system changes its operating conditions, line switching and unpredictable fault location in power system. Therefore, adaptive controller is expected to give good quality of performance under a hardly nonlinearity and complexity of power system [5–6].

Unlike (CPSS), which requires exact a linear plant model for its designing, fuzzy logic controller (FLC) allows to design a controller with unknown or unprecise mathematically model of the nonlinear power system and depending on the experience.

This paper proposed adaptive fuzzy-logic PSS (AFPSS) that grasps the advantages of adaptive of nonlinear fuzzy-logic techniques and overcomes FLC drawbacks. The introduced stabilizer is initialized using the rule-base of a standard FLPSS to guarantee an appropriate performance during the learning step. The rule-base is tuned in real time so that the stabilizer can fit to variuos range operating conditions. The adaptive feature of the introduced stabilizer results in a satisfactory performance using a significantly small rule base due to its tuned parameters as compared to the standard FLPSS.

2. Adaptive Variable Structure FLPSS:

For singleton fuzzifier, ,center average defuzzifier, product inference, and Gaussian membership function, it is easy to shown that [8]

$$v = f(\underline{x}) = \frac{\sum_{l=1}^{M} \theta_i \prod_{i=1}^{p} \mu_{F_i^l}(x_i)}{\sum_{l=1}^{M} \prod_{i=1}^{p} \mu_{F_i^l}(x_i)} \qquad (1)$$

Where M is the number of rules in the FLS and p is the number of inputs to the FLS. θ_l is the centroids of membership functions of the output corresponding to the M rules. Equation (1) can be expressed as

$$v = f(\underline{x}) = \sum_{i=1}^{M} \theta_i \, p_i(\underline{x}) \qquad (2)$$

where $p_i(\underline{x})$ are called fuzzy basis function (FBF) [8] and are given by

$$p_i(\underline{x}) = \frac{\prod_{i=1}^{p} \mu_{F_i^l}(x_i)}{\sum_{l=1}^{M} \prod_{i=1}^{p} \mu_{F_i^l}(x_i)} \qquad (3)$$

Now the FLS can be referred to as a FBF expansion

Consider the nonlinear system

$$y^{(n)} = f(\underline{x}) + bu \qquad (4)$$

Where $f(\cdot)$ is unknown real continuous nonlinear function and b is an unknown constant.

$u \in R$ and $y \in R$ are the input and the output of the system, respectively. $\underline{x} = \left(x, \dot{x}, \ldots, x^{(n-1)}\right)^T \in R^n$ is the system state vector, and $y^{(r)}$ is the rth derivative of y.

The output y is required to follow a reference signal y_m which is selected such that it is derivatives up to the *n*th order exit. Define the tracking error as

$$e = y_m - y, \quad \dot{e} = \dot{y}_m - \dot{y}, \quad e^{(n)} = y_m^{(n)} - y^{(n)}, \ (5)$$

Hence, the tracking error state vector, $\underline{e}$, can be selected as

$$\underline{e} = \begin{bmatrix} e & \dot{e} & \cdots & e^{(n-1)} \end{bmatrix}^T$$

If $f(\underline{x})\ and\ b$ were known, we would choose the feedback control law as

$$u = \frac{1}{b}\left[-f(\underline{x}) + y_m^n + \underline{k}^T \underline{e}\right] \qquad (6)$$

where the design vector $\underline{k}$ is given by $\underline{k}^T = \begin{bmatrix} k_n & k_{n-1} & \cdots & k_1 \end{bmatrix}$. Substituting (6) into (4) leads to

$$y^{(n)} = y_m^{(n)} + \underline{k}^T \underline{e} \qquad (7)$$

Noting the above definition of the tracking error in (5), $\underline{e}$, it is possible to rewrite (7) as

$$e^{(n)} + \underline{k}^T \underline{e} = e^{(n)} + k_1 e^{(n-1)} + \cdots + k_n e = 0 \qquad (8)$$

The characteristic equation of the error model (3.8) is

$$s^n + k_1 s^{n-1} + \cdots + k_n = 0 \qquad (9)$$

The design parameters $k_1, k_2, \cdots, k_n$ are selected such that the roots of (9) are in the left-hand side of the s-plane to ensure stability. Since $f(\underline{x}) \quad and \quad b$ are unknown, the control law (3.6) cannot be implemented. Based on the universal approximation theorem [8,9], there is a fuzzy system that can approximate u; i.e. it is possible to write

$$u \approx \underline{\theta}^T \underline{p}(\underline{x}) \qquad (10)$$

$\hat{\underline{\theta}}$ is the vector estimated of centeroids of the membership functions assigned to u and $\underline{p}(\underline{x})$ is the vector of fuzzy basis functions. The control law (10) is implemented based on an estimate value $\hat{\underline{\theta}}$ of the true values $\underline{\theta}$. Hence, we can write

$$u = u_c(\underline{\theta}, \underline{x}) = \hat{\underline{\theta}}^T \underline{p}(\underline{x}) \qquad (11)$$

Substituting $u_c(\underline{\theta}, \underline{x})$ in (4) leads to

$$y^{(n)} = f(\underline{x}) + b u_c(\underline{\theta}, \underline{x}) \qquad (12)$$

Adding and subtracting bu to (3.12) result in

$$y^{(n)} = f(\underline{x}) + bu + b(u_c(\underline{\theta}, \underline{x}) - u) \qquad (13)$$

Similar to the derivative of (7), it is possible to show that the error model corresponding to the closed loop system (13) is

$$e^{(n)} = -\underline{k}^T \underline{e} + b(u - u_c(\underline{\theta}, \underline{x})) \qquad (14)$$

Eq. (14) can be put in the controllable canonical form by choosing

$$\dot{e}_1 = \dot{e} = e_2,$$

$$\dot{e}_2 = \ddot{e} = e_3,$$

$$\vdots$$

$$\dot{e}_{n-1} = e^{(n-1)} = e_n$$

$$\dot{e}_n = e^{(n)} = -\underline{k}^T \underline{e} + b(u - u_c(\underline{\theta}, \underline{x})) \qquad (15)$$

So, the state space model takes the form

$$\dot{\underline{e}} = A_c \underline{e} + \underline{b}_c (u - u_c(\underline{\theta}, \underline{x})) \qquad (16)$$

where

$$A_c = \begin{bmatrix} 0 & 1 & 0 & \cdots & 0 \\ 0 & 0 & 1 & \ddots & \vdots \\ 0 & \ddots & \ddots & \ddots & 0 \\ 0 & 0 & \cdots & 0 & 1 \\ -k_n & -k_{n-1} & \cdots & -k_2 & -k_1 \end{bmatrix}, \qquad \underline{b}_c = \begin{bmatrix} 0 \\ 0 \\ \vdots \\ 0 \\ b \end{bmatrix}$$

The design parameters $k_1, k_2, \cdots, k_n$ are selected such that the eigenvalues of A_c are located in a pre-specified region of the left-hand side of the s-plane.

The estimate value $\hat{\underline{\theta}}$ is typically based on the second method of Lyapunov to ensure the stability of the adaptive system. To illustrate that, consider the following Lyapunov function.

$$V = \frac{1}{2} \underline{e}^T P \underline{e} + \frac{b}{2} \underline{\phi}^T \Gamma^{-1} \underline{\phi} \qquad (17)$$

where $P \; and \; \Gamma$ are positive definite matrixes and $\phi = \underline{\theta} - \underline{\hat{\theta}}$ is the estimation error. The calculations of $P \; and \; \underline{\phi}$ are shown below. The designer normally picks up the matrix Γ as diagonal matrix that determine the adaptation rate as shown below. The time derivative of V is

$$\dot{V} = \frac{1}{2}(\underline{e}^T P \underline{\dot{e}} + \underline{\dot{e}}^T P \underline{e}) + b\underline{\phi}^T \Gamma^{-1} \underline{\dot{\phi}} \qquad (18)$$

Substituting for $\underline{\dot{e}}$ from (3.16) into (3.18) leads to

$$\dot{V} = \tfrac{1}{2}(\underline{e}^T P A_c \underline{e} + \underline{e}^T P \underline{b_c} \underline{\varphi}^T \underline{p}(\underline{x}) + \underline{e}^T A_c^T P \underline{e} + \underline{b}^T P \underline{e} \underline{\varphi}^T \underline{p}(\underline{x})) + b\underline{\varphi}^T \Gamma^{-1} \underline{\dot{\varphi}} \quad (19)$$

Eq. (3.19) can be simplified to

$$\dot{V} = \frac{1}{2}\underline{e}^T (PA_c + A_c^T P)\underline{e} + \underline{\phi}^T \underline{p}(\underline{x}) \underline{b}_c^T P \underline{e} + b\underline{\phi}^T \Gamma^{-1} \underline{\dot{\phi}} \quad (20)$$

The closed loop system (3.16) is stable if $\dot{V}$ is negative semi-definite. Since A_c has stable eigenvalues, it is true that P is the solution of the algebraic Lyapunov equation

$$PA_c + A_c^T P = -Q \qquad (21)$$

where Q is a positive semi-definite matrix that is arbitrarily chosen by the designer. Select the adaptation law as [10, 11]

$$\underline{\dot{\phi}} = -\frac{1}{b} \underline{b}_c^T P_n \underline{e} \Gamma \underline{p}(\underline{x}) \qquad (21)$$

Where P_n is the second column of the matrix P.

Hence, it is possible to rewrite (19) as

$$\dot{V} = -\frac{1}{2}\underline{e}^T Q e \qquad (22)$$

Eq. (22) clearly shows that the closed-loop system (16) is stable if the adaptation law (21) is employed. To implement (16) and calculate $\hat{\underline{\theta}}$, we assume that the variation of $\underline{\theta}$ is much slower than of $\hat{\underline{\theta}}$ i.e. $\underline{\theta}$ is locally constant [61]. The estimate value $\hat{\underline{\theta}}$ is given by

$$\dot{\hat{\underline{\theta}}} = \frac{1}{b} \underline{b}_c^T P_n \underline{e} \Gamma \underline{p}(\underline{x}) \qquad (23)$$

From 23 we have

$$\dot{\hat{\underline{\theta}}} = \frac{1}{b} \underline{b}_c^T P_n \underline{e} \Gamma \underline{p}(\underline{x})$$

The equivalent sigma-modification law is [11]

$$\mu \dot{\theta}_i = \Gamma_i \underline{e}^T \underline{p}_n \zeta_i(\underline{x}) - \sigma(\theta_i - \theta_i(0)) \qquad (24)$$

The constants μ, Γ_i and σ are design parameters. $\theta_i(0)$ is the initial estimate of θ_i. By selecting $\sigma = 1, \mu \to 0,$ and $\Gamma_i = \bar{\theta}_i / \left\| \underline{e}^T \underline{p}_n \right\| \zeta_i(x)$, we can rewrite (24) as

$$\theta_i = \bar{\theta}_i \operatorname{sgn}(\underline{e}^T \underline{p}_n) + \theta_i(0) \qquad (25)$$

Where $\bar{\theta}_i$ is a constant set by the designer to specify the possible range of variation of θ_i around $\theta_i(0)$. A smaller $\bar{\theta}_i$ reflect more confidence in the corresponding initial value $\theta_i(0)$. To chattering and ensure smooth variation of θ_i, it is common to replace the $\operatorname{sgn}(.)$ function in (25) by the $sat(.)$ function. Hence, the estimater is implemented as

$$\theta_i = \bar{\theta}_i \; sat(\underline{e}^T \underline{p}_n) + \theta_i(0) \qquad (26)$$

The estimates obtained by (25) are used to calculate U_{pss}

Where

$$u = u_c(\underline{\theta}, \underline{x}) = \underline{\hat{\theta}}^T \underline{p}(\underline{x}) \qquad (27)$$

3. Design Procedure Of a Direct Variable-Structure Adaptive Fuzzy PSS

1. Let $x_1 = \Delta\omega$ (speed deviation), $x_2 = \Delta\dot{\omega}$ (speed deviation derivative) be the inputs to the fuzzy basis function (FBF), i.e $\underline{x} = [x_1 \quad x_2]^T = [\Delta\omega \quad \Delta\dot{\omega}]^T$. It is reasonable to choose the generator speed deviation $\Delta\omega$ and its derivative $\Delta\dot{\omega}$ as input signals to the PSS controller, because the aimed is to damping the oscillation of generator speed (system frequency) to zero [11]. Each input is assigned three fuzzy membership functions $N, Z, and\ P$ that stand for the linguistic values negative, Zero, and positive, respectively. Fig. 1 shows the membership functions $N, Z, and\ P$. The membership functions are triangles and equally distributed, the author test unequally distributed membership functions and concentrated within a certain interval as describe in [11], but the author found equally distributed is more effect in our controller specially with triangle shapes. The ranges of membership functions are chosen according to what is expected for maximum and minimum of speed deviation and the derivative of speed deviation

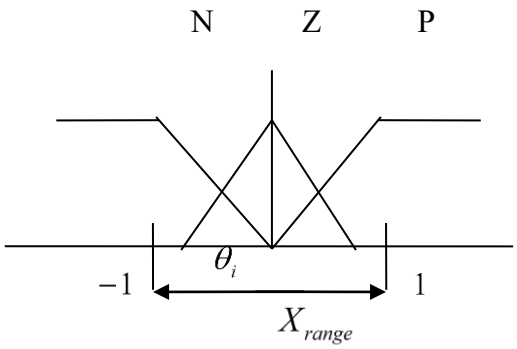

Figure 1: The membership functions used for the AFPSS inputs variables

2. Develop a fuzzy basis function (FBF) rule base with two inputs of speed deviations $\Delta\omega$ and $\Delta\dot{\omega}$, and one output. Set the initial value of $\underline{\theta}$ as initial fuzzy rule base (selected by the designer's experience with help of the table look-up) as in table 1. Apply the adaptation law (26) to compute $\dot{\underline{\theta}}$ online in Table 2 and calculate the FBF from (3) and apply the results to (27) to get the PSS output U_{pss}.

3. Use trial and error method to get the gains of controllers $\underline{k}$ and the second columns of P which is of interest in our calculations.

Table: 1 Initial fuzzy rule base of AFPSS

$\Delta\omega$ / $\Delta\dot{\omega}$	N	Z	P
N	N	N	Z
Z	N	Z	P
P	Z	P	P

Table 2 Tunable fuzzy rule base of AFPSS

$\Delta\omega$ / $\Delta\dot{\omega}$	N	Z	P
N	$\hat{\theta}_1$	$\hat{\theta}_2$	$\hat{\theta}_3$
Z	$\hat{\theta}_4$	$\hat{\theta}_5$	$\hat{\theta}_6$
P	$\hat{\theta}_7$	$\hat{\theta}_8$	$\hat{\theta}_9$

4. Simulation Results

Nonlinear power system which is used in simulation studies consists of single machine infinite bus power systems. The performance of proposed (AFPSS) and compared with CPSS as shown in Fig. 2, is

evaluated by acting the large disturbance in transmission line at 2 sec and cleared ant 2.133 sec.

The system performance tracking index is characterized by *ISE* as:

$$ISE = \int e^2(t)dt \qquad (28)$$

where e is the out signals deviation

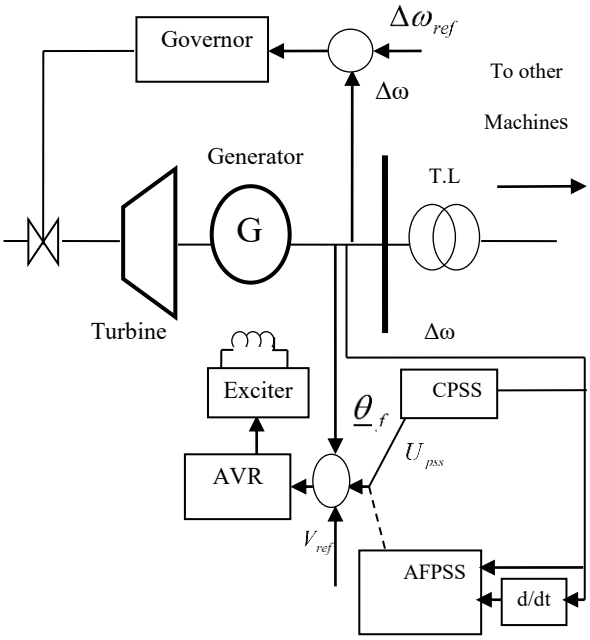

Figure 2: Power system model used in study of one Machine

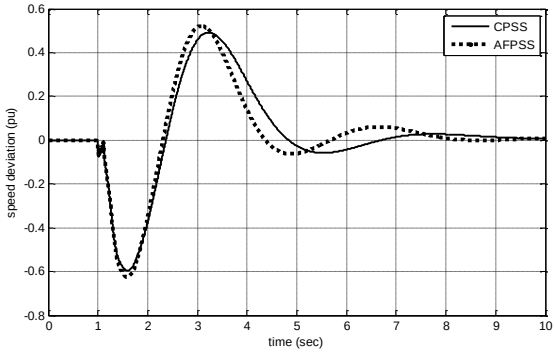

Figure 3: speed deviation response for Gen. (1)

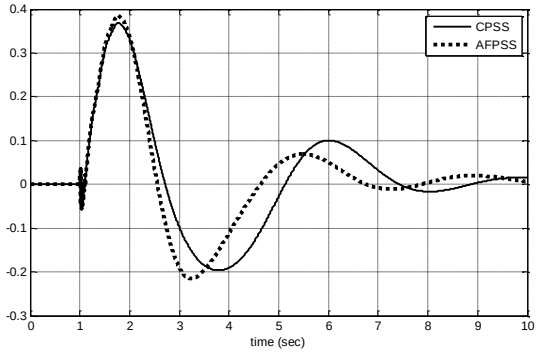

Figure. 4: speed deviation response of operating condition (0.4 pu)

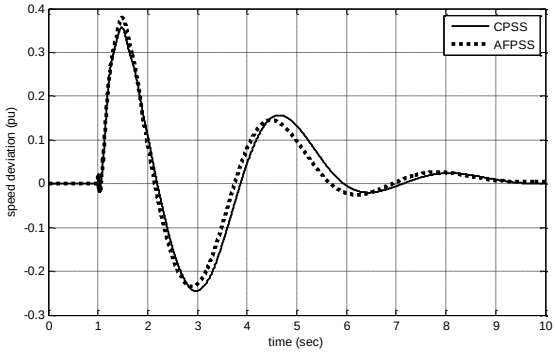

Figure 5: speed deviation responseof operating condition (0.8 pu)

Table 3 Index equation (28)

	Speed Deviation
CPSS	0.49
AFPSS	0.32

5. Conclusion:

In this paper, dynamic behavior single machine infinite bus installed with a conventional power system stabilizer (CPSS) is investigated under 3-phased fault. Proposed Adaptive Fuzzy based power are designed to improve damping local mode of oscillations following three phase faults that occurs at 1 sec. and cleared at 1.13 sec.

The simulation results of the proposed AFPSS applied to single machine infinite busprovides the smallest ISE index compared with CPSS. Therefore, results it is recommended to be considered in further and extended studies.

References:

1. Ritu Jain and Shruti Choubisa " Power System Stability Enhancement Using Fuzzy Based Power System Stabilizer" International Journal of Research and Scientific Innovation (IJRSI) | Volume III, Issue VII, July 2016 | ISSN 2321-2705.
2. EmiraNechadi, Mohamed Naguib Harmas, Najib Essounbouli, Abdelaziz Hamzaoui " Adaptive Fuzzy Sliding Mode Power System Stabilizer Using Nussbaum Gain" International Journal of Automation and Computing, 10(4), August 2013, 281-287 DOI: 10.1007/s11633-013-0722-0.
3. E. Nechadi and M.N. Harmas " Power System Stabilizer Based on Global Fuzzy Sliding Mode Control" balkan journal of electrical & computer engineering, 2013, Vol.1, No.2.
4. A.R. Roosta and H. Khorsand " An Adaptive Fuzzy-Logic Stabilizer for Single and Multi-Machine Power Systems" World Applied Sciences Journal 12 (4): 385-394, 2011 ISSN 1818-4952. IDOSI Publications, 2011.
5. A. Jamal AND R.Syuthputra " Design of PSS Based on Adaptive Neuro-Fuzzy Method" Proceedings of International Seminar on Applied Technology, Science, and Arts (3rd APTECS), Surabaya, 6 Dec. 2011, ISSN 2086-1931.
6. E. Nechadi " Adaptive Fuzzy Type-2 Synergetic Control Based on Bat Optimization for Multi-Machine Power System Stabilizers" Engineering Technology and Applied Science, Vol. 9 No. 5 (2019): October, 2019

7. T. Hussein Elmenfy " Different Trends on Power System Stabilizer " International Journal of Power Systems http://www.iaras.org/iaras/journals/ijps.

8. A. L. Elshafei, K. A. El-Metwally and A. A. Shaltout " A Variable-Structure Adaptive Fuzzy-Logic Stabilizer for Single and Multi-Machine Power Systems" *Control Engineering Practice, vol. 13, no. 4, pp 413-423, 2004.*

9. L. X. Wang " A Course in Fuzzy Systems and Control" *Prentice-Hall PTR, Upper Saddle River: NJ, 1997.*

10. X. Zheng, H. Zaman, X. Wu, H. Ali, S. Khan "Direct fuzzy logic controller for voltage control of standalone three phase inverter" International Electrical Engineering Congress (IEECON)2017.

11. Jerry Mendel, Hani Hagras, Woei-Wan Tan, William W Melek, Hao Ying "Introduction to type-2 fuzzy logic control: theory and applications, 2014/6/16, John Wiley & Sons.

12. L, Xin, C. Wei " Aprroximation Accuracy of Some Neuro-Fuzzy Approaches" IEEE Transactions on Fuzzy Systems vol. 8, No. 4, pp470-477, August, 2000.

Journal of Total Science
Volume (6), Issue (24) (June. 2023)
ISSN: 2518-5799

مجلة العلوم الشاملة
المجلد (6)، العدد (24)، (يونيو2023)
ردمد: 2518-5799

A COMPARISON BETWEEN IMAGE SEGMENTATION MODELS WITH DIFFERENT METHODS

هبة مصطفـى علـي أبو عائشة
المعهد العالي للعلوم والتقنية الزهراء

سليمان عبد الجليل العارف المودي
المعهد العالي للعلوم والتقنية صبراتة

الملخص

تجزئة الصورة هي احدى الطرق الرئيسية المستخدمة في معالجتها والتي تعتمد بشكل أساسي على تقسيم الصورة الى مقاطع متساوية بمكن تحليلها وربطها.

يقدم هذا البحث طريقة كنتورية نشطه مستوحاة من مصفوفة هس والقيم الذاتية. تعطي الطريقة المطورة كفاءة مختلفة لطريقة الكنتور النشط مع طريقة تحويل فورية. علاوة على ذلك يتم تحويل صورة الادخال الى مجال التردد ويتم اجراء جميع حسابات مصفوفة هس والقيم الذاتية الضرورية في هذا المجال. تتم مقارنة الطريقة مع الطرق المطورة الأخرى في المجال حيث تظهر النتائج أن التقنية المستهدفة لها عدد تكرارات ومدة معالجة مماثلة للطرق الفعالة ولكن لديها القدرة على زيادة الدقة.

تظهر المقارنة التي تم اجراؤها بناءً على رقم الجدارة ان الطريقة يمكن ان تسفر عن نتائج أفضل في أوقات وتكرارات معالجة أقصر.

Abstract

Image segmentation is one of the main methods that are used in image processing, which mainly depends on dividing the picture into equal segments that can be analyzed and correlated. This research presents an active contour method that is inspired by Hessian matrix and eigenvalues. The developed method gives a different competence to the active contour method with the Fourier transform. Moreover, the input image is transformed into the frequency domain and all necessary Hessian and eigenvalue calculations are made in this field. The method is compared with other developed methods in the domain, where the results show that the targeted technique has a similar iterations and processing duration of other efficient methods but has the potential to increase accuracy. The comparison performed based on figure of merit (FOM) shows that the method can yield better results in shorter processing times and iterations.

Keywords: image processing; Hessian Matrix; segmentation

1. INTRODUCTION

Image segmentation is widely used in computer vision and image processing. Meaningful information can be extracted by segmentation in special areas of image processing applications. The active contour method developed by Kass et al. [1] is among the popular image segmentation methods and produces effective results in very difficult problems. The active contour method is a method that finds different objects by detecting the edges of objects in images. In this method, a band is first created around the objects that surrounds them. Parallel to the progress of the algorithm, the points forming the strip approach towards the object and stand on the edges of the object. Thus, the edge regions of the objects are detected.

Active contour models are generally examined in two main classes: edge-based models [2] and region-based models [3, 4]. Among the edge-based methods, the most well-known is the geodetic active contour method [5]. In this method, the edges are determined according to the gradient size. However, this method is affected by noise. Region-based active contour methods generally use the level set method [6, 7]. The CV method is the most well-known among these methods [8]. In these methods, the energy remaining in the inner and outer shadow of the curve is defined. The curve obtained when the energy reaches the minimum value is defined as the boundary of the object. Approaches have been developed to improve the energy calculations in this method [9]. Thus, the noise sensitivity and operating speed of the CV method are improved. Moreover, studies that can perform soft contour segmentation have been developed in order to obtain better segmentation in images where the

contour inner region is irregular [10]. In another study, modified Heaviside and Dirac delta functions were used to update the level set function [11]. Thus, especially the working speed of region-based segmentation methods has been improved. In an active contour method designed to reduce the noise effect in the edge regions, the regional similarity factor was developed [12]. Thus, the similarity values of neighboring pixels were analyzed, and the noise components were eliminated. A cascade learning method has been developed to detect and segment regions with different appearance behaviors in the image [15]. In this method, the shape information of the region of interest and the probabilistic model of the appearance information of the same region are used together in the level set function. However, this method is color dependent and does not give the desired result in different color regions that may be present in the images.

In the above-mentioned literature studies, the weaknesses of the methods against noise, high working times and low success in color differences stand out as the main deficiencies. Based on these issues, a new active contour method has been developed in this study, which is fast, has high segmentation accuracy and can obtain smooth object boundaries. In the developed region-based segmentation method, the Fourier transform was integrated into a method previously developed in the literature, and the method was transferred to the frequency domain. Thus, the behavior of the level cluster function of the method is improved by detecting the important regional frequency components that cannot be obtained with the eigenvalue matrix in some images, but which are necessary.

2. HESSIAN MATRIX AND EQUITY BASED ACTIVE CONTOUR METHOD

Instead of gradient information used in derivative calculations in images, second-order derivative calculations can be used to obtain information expressing changes such as edges and vertices. From this point of view, effective segmentation methods have been developed with the eigenvalue information obtained by calculating the Hessian matrix of the image instead of the gradient calculation among the active contour methods [13, 14]. In this method, which is based on using the eigenvalue information, the density information of the inner and outer contours is calculated using the level set method. For this, first and second order derivatives of an I image are calculated, and the Hessian matrix is calculated as follows [15]:

$$H(x,y) = \left(\frac{\partial^2}{\partial x^2} I(x,y) \frac{\partial^2}{\partial x \partial y} I(x,y) \frac{\partial^2}{\partial x \partial y} I(x,y) \frac{\partial^2}{\partial x^2} I(x,y)\right) = \left[D_{xx} D_{xy} D_{xy} D_{yy}\right]$$

Where, D_{xx}, D_{yy} and D_{xy} denote the second-order horizontal, vertical, and diagonal derivatives of the image, respectively. Using the calculated Hessian matrix, the eigenvalue matrices of the image are calculated as follows:

$$\lambda_1 = \frac{1}{2}\left(D_{xx} + D_{yy} - \sqrt{-2\,D_{xx}D_{yy} + {D_{xx}}^2 + 4\,{D_{xy}}^2 + {D_{yy}}^2}\right.$$

$$\lambda_2 = \frac{1}{2}\left(D_{xx} + D_{yy} - \sqrt{-2\,D_{xx}D_{yy} + {D_{xx}}^2 + 4\,{D_{xy}}^2 + {D_{yy}}^2}\right.$$

Where, λ_1 and λ_2 are eigenvalue matrices. Once this information has been calculated for the image, it is used to minimize the following energy function:

$$E(c_1, c_2, C) = \int_{inside(c)} |I(x) - c_1|\, dx + \int_{outside(c)} |I(x) - c_2|\, dx \quad , \quad x \in \Omega$$

Where, (x):$\Omega \rightarrow \mathbb{R}$ and C:$[0,1] \rightarrow \Omega$ define a parameterized planar curve. The C contour divides the I image into two non-overlapping regions. By minimizing the energy function in terms of c_1 and c_2 terms, optimal c_1 and c_2 information is obtained. Thereafter, the eigenvalue matrices of the image are integrated into the energy function as follows, and the active contour curve expressing the correct object boundary is obtained:

$$E(c_1, c_2, C) = \left(\int_{inside(c)} \frac{I(x) - \frac{c_1 + c_2}{2}}{\left(\left| I(x) - \frac{c_1 + c_2}{2} \right| \right)} dx + \int_{outside(c)} \frac{I(x) - \frac{c_1 + c_2}{2}}{\left(\left| I(x) - \frac{c_1 + c_2}{2} \right| \right)} dx \right) \left| eig\left(H(I(x)) \right) \right|$$

Where, $|e(\mathcal{H}(I(x)))|$ represents the eigenvalues of the Hessian matrix of the image I. By using the eigenvalue information in the energy function, the (c_1, c_2, C) function is minimized according to the Lipchitz function (ϕ), so that the gradient descent flow is calculated with the following expression:

$$\frac{\vartheta\phi(x,t)}{\vartheta t} = H\left(spf\left(I(x)\right).\left|eig\left(H\big(I(x)\big)\right)\right|\right)$$

Where, the spf function helps to calculate the object edges using the initial contour, while $|e(\mathcal{H}(I(x)))|$ With the expression, it is aimed to reveal especially the object edges by using the size information of the eigenvalue matrices. Because edge and corner information of different objects in the image are effectively revealed with eigenvalue information. Since the pixel changes are given to the energy function with eigenvalues, rapid convergence of the edge regions of the contour is ensured during the iterative progression of the initial active contour.

This method produced very good results on many images. However, it cannot give the desired results in some images where the differences within the class are small, and the object boundaries are noisy. In addition, it is seen that the frequency domain representation information of the edge regions of the objects is not included in the iterative contour finding process. For this reason, this developed method does not give the desired result in some images.

3. RESEARCH METHOD

The Fourier transform is used to convert a signal in the time domain to the frequency domain [16]. Thus, it is aimed to extract meaningful information by providing the understanding of the signal. Being able to analyze a signal independently of parameters such as translation and scaling is one of the important advantages of the Fourier transform. Similarly, by calculating Fourier transforms in images, local and regional pixel behaviors in the frequency domain can be analyzed. Fast Fourier

transform (FFT) is used to make Fourier transform more efficient and faster [17].

The Fourier transform of an I input image of size $M \times N$ is calculated using Equation 7 as follows:

$$F(u,v) = \sum_{x=0}^{M-1} \sum_{y=0}^{N-1} I(x,y) \times e^{\frac{-j2\pi(ux+vy)}{N}}$$

The pixels of the image are converted into the frequency domain with the Fourier transform. In the studies carried out, important information in the images can be extracted and analyzed by using both the frequency spectrum and the phase spectrum obtained with the Fourier transform.

In this study, it is aimed to bring an important innovative approach to the active contour method. In this context, it is aimed to actively include the frequency components of the regions to be segmented into the energy function by calculating the one-time FFT of the image to be segmented. Thus, instead of calculating the Hessian matrix and eigenvalues of the raw input image, the Hessian matrix and eigenvalues of the Fourier transform of the input image are calculated. Thus, it is aimed to develop a method that is minimally affected by situations such as rotation, overlap and noise that may occur in the image. The basic steps of the developed method are as follows:

Step 1: The level set function is started by defining it as follows:

$$\phi(x, t=0) = \{1, \quad x \in \Omega_0 - 1, \quad x \in \Omega - \Omega_0$$

Where, Ω_0 represents a subset of the image Ω.

Step 2: Calculate the FFT of the input image $F\ (u,\ v)$.

Step 3: Using Equation 1, the Hessian matrix of $F\ (u,\ v)$ is calculated.

Step 4: Hessian's eigenvalue matrices λ_1 and λ_2 are calculated.

Step 5: The magnitude information of the eigenvalues is calculated by the expression:

$$\left|eig\left(H(F(u,v))\right)\right| = \sqrt{{\lambda_1}^2 + {\lambda_2}^2}$$

Step 6: The energy function $E\ (c_1,\ c_2,\ C)$ is minimized iteratively as sub-operations.

Step 6.1: $|\phi k+1-\phi k|>0$, where k is the number of iterations.

Step 6.2: The functions $c_1(\phi)$ and $c_2(\phi)$ are calculated.

Step 6.3: The spf function is calculated by the expression:

$$spf\big(I(x)\big) = \frac{I(x) - \frac{c_1+c_2}{2}}{\left(\left|I(x) - \frac{c_1+c_2}{2}\right|\right)}$$

Step 6.4: The level set function is evaluated. In this study, the level set function is arranged as follows and the Fourier transform $(u,\ v)$ information of the image is used iteratively in the level set function:

$$\frac{\vartheta\phi(x,t)}{\vartheta t} = H\left(spf\left(I(x)\right).\left|eig\left(H(F(u,v))\right)\right|\right)$$

Step 6.5: The (x) function is updated.

Step 7: If the level set function is optimized at the desired level, the iteration is terminated.

The most important difference in the basic steps of the proposed method is that the Fourier transform $(u,)$ information is integrated into the level set function and thus the frequency components of the image are used in the energy minimization process. Thus, derivative-based variation information of local pixel behavior is made in frequency domain instead of spatial domain. By moving the input image to the frequency domain, the changes in the pixel density information occurring in the edge regions of the objects are precisely coded. The energy in the inner and outer regions of the active contour is calculated quickly and the spf function is operated in a safer range. Thus, the level set function reached the optimal values quickly.

The hybrid use of Fourier transforms, and eigenvalue calculations is considered an innovative perspective in the active contour literature. In addition to the features of the Fourier transform, the fact that the eigenvalues yield effective results regardless of rotation and scaling has provided a remarkable efficiency. In this situation, segmentation results with desired accuracy could be obtained especially at concave and convex object boundaries. The geometrically flat, concave, convex or valley appearance of the object edges regions did not affect the operation of the method. Because the eigenvalues usually have geometric properties that can distinguish the pixel density change in such regions from the background and neighboring regions.

4. EXPERIMENTAL RESULTS

In this section, the segmentation results of the FFT-based active contour model developed are compared with other methods. Segmentation accuracy was used as an evaluation criterion. The images used are medical images and some other known images that are frequently used in active contour studies. The proposed method is compared with two different current methods. The first method is the region-based active contour method, the details of which the developed method improves the segmentation performance by addressing it [18]. The second method is called the LIF method and is based on regional contour energy calculation [19]. FOM calculation known as Figure of Merit was used to compare the results of segmentation methods as metric [20]. If the FOM value is 1, it means that the segmentation method produced the same result as the ideal segmentation and obtained the most accurate result. In the relevant tables where the metric results are compared, the best values are indicated in bold font.

The application was carried out on a color image. Segmentation results are shown in Figure 1. The proposed new method improves the results of the existing Hessian-eigenvalue-based method developed with FFT. It was able to accurately detect the inner and outer shadow boundaries of the number 4 in the image. In particular, the detection of outer zone contours is an indication that spf and energy function work more effectively with frequency domain information. The original Hessian-eigenvalue-based method, on the other hand, found the outer region boundaries as double contours. The LIF method, on the other hand, produced the worst results in terms of both time and segmentation

accuracy. Both the inner zone and outer zone boundaries are jagged and inaccurate.

Original

LIF

Original Hessian-Eigenvalue Method

Proposed FFT based Hessian-Eigenvalue Method

Figure 1. Segmentation results of methods for color image

Active contour-based segmentation methods calculate these contours by minimizing the energy function iteratively. Thus, in comparison studies, how many iterations and how long (seconds) the methods complete the active contour generation process is also an important parameter.

Moreover, FOM results are also included in order to measure the similarity of the generated segmentation results with the real segmentation as metric. Therefore, the iteration numbers and working times of the methods for the results seen in Figure 1 are given in Table 1. In order for the LIF method to produce the best results, the optimal iteration number is fixed at 700. However, it did not achieve the desired results. Although the original Hessian-eigenvalue method has a lower iteration number and running time than the new developed method, it has a lower FOM value in terms of segmentation accuracy.

Table 1. Comparison of iteration numbers, running times and FOM values of the methods for the results in Figure 1

Method	Number of Iterations	Duration (sec)	Figure of Merit (FOM)
LIF	700	7.952	0.729
Original Hessian-Eigenvalue Method	**3**	**0.168**	0.147
Proposed FFT based Hessian-Eigenvalue Method	4	0.207	**0.735**

5. CONCLUSION

In this study, an active contour method, which uses the existing Hessian matrix and eigenvalue information working in the spatial domain, has been developed to give a different competence to the active contour method with

the Fourier transform. In the developed method, the input image is transformed into the frequency domain and all necessary Hessian and eigenvalue calculations are made in this field. Thus, it is aimed that the *spf* and energy functions will produce effective results with the pixel density information obtained from the frequency components of the image. The developed method was able to detect the object boundaries better than the original method. In particular, the over-segmentation problem has been resolved. Although the new method is relatively costly compared to the original method in terms of the number of iterations and running time, the segmentation accuracy is better. According to the comparison results, the new method outperformed the LIF method in the literature in terms of all parameters.

However, the developed method has partial deficiencies in distinguishing weak object edges from the background. It is thought that this deficiency will be eliminated by the analytical pixel-based interpretation of the eigenvalue information at the object edges. It is planned to carry out studies in this direction in the future. In addition, it is aimed to examine the behavior of other frequency domain transformations related to Hessian and eigenvalue calculations.

REFERENCES

[1] M. Kass, A. Witkin and D. Terzopoulos, "Snakes: Active Contour Models," *International Journal of Computer Vision,* vol. 1, no. 4, pp. 321-331, 1988.

[2] F. Pierre, M. Amendola, C. Bigeard, T. Ruel and P.-F. Villard, "Segmentation with Active Contours," *Image Processing On Line,* vol. 11, pp. 120-141, 2021.

[3] F. Akram, M. A. Garcia and D. Puig, "Active contours driven by local and global fitted image models for image segmentation robust to intensity inhomogeneity," *PLOS ONE,* vol. 12, no. 4, 2017.

[4] W. Chen, C. Liu and B. Pan, "An Improved Active Contour Model Based on Local Information," *Open Access Library Journal,* vol. 8, pp. 1-10, 2021.

[5] J. Ma, D. Wang and X.-P. Y. X. Wang, "A Characteristic Function-based Algorithm for Geodesic Active Contours," *SIAM Journal on Imaging Sciences,* vol. 14, no. 3, 2021.

[6] H. Yu, P. Sun, F. He and Z. Hu, "A weighted region-based level set method for image segmentation with intensity inhomogeneity," *PLOS ONE,* vol. 16, no. 8, 2021.

[7] H. Min, L. Xia, J. Han, X. Wang, Q. Pan, H. Fu, H. Wang, S. Wong and H. Li, "A multi-scale level set method based on local features for segmentation of images with intensity inhomogeneity," *Pattern Recognition,* vol. 91, pp. 69-85, 2019.

[8] T. F. Chan and L. A. Vese, "Active contours without edges," *IEEE Trans Image Processing,* vol. 10, no. 2, pp. 266-277, 2001.

[9] E. S. Brown, T. F. Chan and X. Bresson, "Completely Convex Formulation of the Chan-Vese Image Segmentation Model," *International Journal of Computer Vision,* vol. 98, pp. 103-121, 2012.

[10] Z. Hongmei and W. Mingxi, "Improved Mumford–Shah Functional for Coupled Edge-Preserving Regularization and Image Segmentation," *EURASIP Journal on Applied Signal Processing,* pp. 1–9, 2006.

[11] R. V. Menon, S. Kalipatnapu and I. Chalrabarti, "High speed VLSI architecture for improved region based active contour segmentation technique," *Integration,* vol. 77, pp. 25–37, 2021.

[12] S. Niu, Q. Chen, L. de Sisternes, Z. Ji, Z. Zhou and D. L. Rubin, "Robust noise region-based active contour model via local similarity factor for image segmentation," *Pattern Recognition,* vol. 61, pp. 104–119, 2017.

[13] O. Pankratov and A. Kuvshinov, "General formalism for the efficient calculation of the Hessian matrix of EM data misfit and Hessian-vector products based upon adjoint sources approach," *Geophysical Journal International,* vol. 200, no. 3, pp. 1449–1465, 2015.

[14] X. Li, X. Wang, X. Cheng, H. Tan and X. Li, "Multi-Focus Image Fusion Based on Hessian Matrix Decomposition and Salient Difference Focus Detection," *Entropy,* vol. 24, no. 11, 2022.

[15] J. Fan, X. Zong, H. Tang, X. Bi, B. Xiao and W. Li, "HessHist: A Hessian-matrix weighted histogram for image contrast enhancement," *IET Image Processing,* vol. 16, no. 7, pp. 1831–1845, 2022.

[16] J. W. Cooley and J. W. Tukey, "An algorithm for the machine calculation of complex Fourier series," *Mathematics of Computation,* vol. 19, no. 90, pp. 297–301, 1965.

[17] P. Duhamel and M. Vetterli, "Fast fourier transforms: A tutorial review and a state of the art," *Signal Processing,* vol. 19, no. 4, pp. 259–299, 1990.

[18] X. Yin, B. Ng, Y. Zhang and D. Abbott, "Accurate Image Analysis of the Retina Using Hessian Matrix and Binarisation of Thresholded Entropy with Application

of Texture Mapping," *PLOS ONE,* 2014.

[19] K. Zhang, H. Song and L. Zhang, "Active contours driven by local image fitting energy," *Pattern Recognition,* vol. 43, no. 4, pp. 1199-1206, 2010.

[20] I. E. Abdou and W. K. Pratt, "Quantitative design and evaluation of enhancement/thresholding edge detectors," *Proceedings of the IEEE,* vol. 67, no. 5, pp. 753-763, 1979.

Journal of Total Science
Volume (6), Issue (24) (June. 2023)
ISSN: 2518-5799

مجلة العلوم الشاملة
المجلد (6)، العدد (24)، (يونيو2023)
ردمد: 2518-5799

A CORRELATIONAL STUDY ON THE EFFECT OF NATINAL CRISS ON THE MENTAL HEALTH OF THE STUDENTS OF THE FACULTY OF DENTAL AND ORAL SURGURY, ATTAHADI UNIVERSITYAND THEIR ACADEMIC PERFORMANC ".

Thabet Al-hani Mohamed ,**Attallah Ghareba**

Faculty Of Science And Medical Technology/Tripoli, Attahadi Medical University

ABSTRACT:

The study aimed to determine the relationship of the effects of the national crisis on the mental of the students and their academic performance. Specifically, this study aimed to answer the following questions: 1.) What are the effects of the National crisis on the mental Health of thestudents? 2.) What are the level of academic performance of the students? 3.) Is There a significant relationship between the effect of the national crisis on the mental health status of the students at the Faculty of Pharmacy and their academic performance? The finding that the researcher was able to extract from the study were: 1) The effects of the National crisis on the mental health of the students disclosed the verbal interpretation of "Rarely ". Indeed, it can be said that the mental health of the students was not that greatly affected. 2) The academic performance of the students disclosed that Year levels 1 and 3 have a verbal interpretation of "Good ", and Year level 2 as "Fair". Though the academic performance of the students doesn't show a verbal interpretation of weak or very weak, it is still worthwhile to not that none have reached the very good and the excellent.So we could still say that there is a need for the students coping strategies be enhanced for them to reach their maximum potentials with their academic performance. 3) Statistical evidence shows that an r= 0.03 shows a weak positive relationship among variables. Though it's not that high, indeed, the mental health of the students can be a predictor to their academic Performance.

KEY WORDS:National Crisis, Mental Health Academic Performance

INTRODUCTION:

Among the consequence of war, the negative impact it had on the mental health of the people of the society in general has been catastrophic. War destroys communities and families and lives. It leads to widespread human suffering and population displacement, it often disrupts the development of the social and economic fabric of nations. It disturbs and interrupts people's ability to live in peace and harmony. It corrupts nations and ruinsgenerations and effects the youth especially on a large study have shown that conflict situations cause more mortality and disability.

The effects of war include long-term physical and psychological harm to children and adults as well as reduction in material and human capital. Death s a result of wars is simply the "tip of the iceberg ". Other consequences, besides death, are not well documented. They include endemicpoverty,malnutrition,disability,economic/social decline and psycho-social illness, to mention only a few.

It becomes very difficult for children to grow up normally in an environment filled with fear and death and hopelessness and still manage to find a way to live their lives to its full power and money and status, the balance of peace and well – being will be disrupted and although the situation in Libya has been extremely difficult to live with and to handle, the youth of our society are still fighting through it all to have a good chance at education and to achieve theirgoal of beingapartofthenextgenerationthat would build a better future for our country.

The impact of Libya's nine-year war on civilians is "incalculable ", a UN official has said, with rising casualties and nearly 900,000 people now needing assistance.

The impact of wars on the mental health of the civilian population is one of the most significant studies of the general population show a definite increase in the incidence and prevalence of metal disorders. Women are more affected than men. Other vulnerable groups are children, the elderly and the disabled. Prevalence rates are associated with the degree of trauma, and the availability of physical and emotional support. The use of cultural and religious coping strategies is frequent in developing countries.[1]

The impact of wars on the mental health of the civilian population is one of the most significant studies of the general population show a define increase in the incidence and prevalence of metal disorders. Women are more affected than men. Other vulnerable groups are children, the elderly and the disabled. Prevalence rates are associated with the degree of trauma, and the availability of physical and emotional support. The use of cultural and religious coping strategies is frequent in developing countries.

At this juncture, the researchers are bent on pursuing this study entitled, "A Correlational Study on the Effect of National Crisis on the Mental Health of the Students of the Faculty of Dentistry, Attahadi University, their Academic Performance".

METHODS:

ThisstudyemployedtheDescriptiveCorrelationalmethodofresearch.The respondents ofthisstudywerethestudentsofAttahadiUniversityfromtheFaculty of Pharmacy, which is composed of 40 students. Out of the 59 total population fourty (40) samples formed the respondents. The researchers made use of Triangulation in research where we employed a combination of two (2) Sampling Techniques. The convenience or accidental sampling and purposive sampling to ensure validity of data for the academic performance. Those students present during the actual data collection were the one who formed the respondents of the study.

The researcher made use both of primary data and secondary data as well as a tool in collecting data. The questionnaire with the use of Likert scale measures the effect of the national crisis on the mental health of the students. The researchers also made use of the secondary data to measure the academic performance of the respondents. The general weighted average of the students for each year level was taken into account to measure the second variable of the study.

Communication was sent to the Dean of the Attahadi University, Faculty of Pharmacy, for the approval of the conduct of data collection. After the permission was sought, the researchers proceed on the actualconductofdatacollectionbydistributingquestionnaires to the respondents and retrieving it on the same day. For the secondary data, a communication wassenttotheDeanto seek perusal on the retrievalofgrades. Afterthedatawasretrieved, it was treated statistically.

RESULTS:

Detailed scrutiny of Table 1 reveals an overall mean of 3.83 which have a verbal interpretation of “Rarely ”.

Table 1

Mean and verbal interpretation of the effects of the National CrisisOn the Mental Health of the Students

Indicators	Mean	Verbal Interpretation
1. Ifelt sad, unhappy or depressed.	2.85	Sometimes
2. I feel lethargic, apathetic or as if I have no energy.	2.7	Sometimes
3. I feel hopeless about the future.	4.22	Never
4. I feel lonely, isolated or alone.	3.92	Rarely
5. I have trouble sleeping.	3.07	Rarely
6. I sleep too much.	3.55	Rarely
7. I have no appetite.	4.12	Never
8. I overeat.	3.14	Rarely
9. I feel unproductive or get distracted easily at work.	3.57	Rarely
10. I have trouble focusing on projects, work or activities.	3.3	Rarely
11. Activities or work no longer interest me.	3.69	Rarely
12. I have trouble getting along with family, friends, co workers.	4.49	Never
13. I feel tense or nervous.	2.54	Sometimes
14. I feel agitated, angry or irritable.	2.77	Sometimes
15. I think about hurting myself.	4.55	Never
16. I consider suicide.	4.87	Never
17. I drink or do drugs to escape or dull the pain.	4.8	Never
18. I binge drinks (more than 5 drinks in 1 hour)	4.94	Never
19. People express concern about my drinking or drug use.	4.8	Never
20. I have had trouble at work/school due to alcohol or drugs.	4.8	Never

Overall			3.83	**Rarely**
Legend:	4.1 – 5.0	Never		
	3.1 – 4.0	Rarely		
	2.1 – 3.0	Sometimes		
	1.1 – 2.0	Mostly		
	0.1 – 1.0	Always		

Detailed Scrutiny of Table 2 reveals an overall mean of 68.9 which have a verbal interpretation of "Good ".

Table 2

Mean and Verbal interpretation of the extent Of the First Year student's level of academic performance As measured by their general weighted average

Indicator	Mean	Verbal Interpretation
First Year weighted average grade	68.9	Good

Legend:	100-85	Excellent
	84.9-75	Very Good
	74.9-65	Good
	64.9-50	Fair
	49.9-35	Weak

34.9-0 Very weak

Detailed Scrutiny of Table 3 reveals an overall mean of 68.9 which have a verbal interpretation of "Fair ".

Table 3

Mean and Verbal interpretation of the extent of the Second Year student's level of academic performance as measured by their general weighted average

Indicator	Mean	Verbal Interpretation
Second Year weighted average grade	63.76	Fair

Legend:
100-85 Excellent
84.9-75 Very Good
74.9-65 Good
64.9-50 Fair
49.9-35 Weak
34.9-0 Very weak

Detailed Scrutiny of Table 4 reveals an overall mean of 74.08 which have a verbal interpretation of "Good ".

Table 4

Mean and Verbal interpretation of the extent of the Third Year student's level of academic performance as measured by their general weighted average

Indicator	Mean	Verbal Interpretation
Third Year weighted average grade	**74.08**	**Good**

Legend:

100-85	Excellent
84.9-75	Very Good
74.9-65	Good
64.9-50	Fair
49.9-35	Weak
34.9-0	Very weak

Table 5

Mean and Verbal Interpretation of the summary of the extent Of the student's level of academic performance as measured by their general weighted average

Year Level	Mean	Verbal Interpretation
1	68.9	Good
2	63.76	Fair
3	74.08	Good

Legend:		
	100-85	Excellent
	84.9-75	Very Good
	74.9-65	Good
	64.9-50	Fair
	49.9-35	Weak
	34.9-0	Very weak

Detailed analysis of Table 6reflecting the relationship between the two variables of the study which reveals a positive weak correlation.

Table 6

Pearson Momentum Correlation between the Effects of the National Crisis on the mental health Of the students and the student's level academic Performance.

Variables		
National Crisis effected on the Mental health of students (X)	Pearson Correlation Level of Sig N	0.03 .26 40
Academic Performance In Major Nursing Subjects (Y)	Pearson Correlation Level of Sig N	0.03 .26 40

There was a positive weak correlation between the two variables, r=0.03 n=40, p=.26

DISCUSSION:

BasedontheresultsfromTable1,theAttahadiUniversity,FacultyofPharmacy students from Levels 1-3 effects of National Crisis on the mental health of the students falls with the category of "Rarely". It is worthwhile to note that despite the crisis that the students are currently experiencing, the results showed that they were able to adapt and was rarely affected. The students were able to develop some sense of resiliency.

Accordingtosomestudies,mentalhealthofadolescentshastakenconsiderable attention worldwide, because of a dramatic upward trend in suicide. More than twenty percent of adolescentsintheU.S.haveamentalhealthdisorder,andoneinfiveofthemareaffected by a mental health problem, which is estimated to account for a larger burden of disease than any other class of health conditions. [2]

Most of the mental health problems are related to deprivation, poverty, inequality and other social and economic determinants of health. Economic crises are therefore times of high risk to the mental well-being of the population and of the people affected and their families.[3]

Symptoms of a mental illness can be better or worse at times. This happens when people are doing their best to manage their illness, too. Experiencing worsening symptoms for a short period of time is a normal part of the recovery process. Sometimes we need outside help when symptoms become worse. Some people may also need urgent emergency help if they're at risk of hurting themselves or others. Fortunately, we can take steps to help control mental health crises and emergencies.[4]

Most people affected by emergencies will experience distress (e.g. feelings of anxiety and sadness, hopelessness, difficulty sleeping, fatigue, irritability or anger and/or aches and pains). This is normal and will for most people improve over time. However, the prevalence of common mental disorders such as depression and anxiety is expected to more than double in a humanitarian crisis.[5]

The WHO stress that mental health is "more than just the absence of mental disorders or disabilities." Peak mental health is about not only

avoiding active conditions but also looking after ongoing wellness and happiness.[6]

Multiple social, psychological, and biological factors determine the level of mental health of a person at any point of time. For example, violence and persistent socio-economic pressures are recognized risks to mental health. The clearest evidence is associated with sexual violence.

Poormentalhealthisalsoassociatedwithrapidsocialchange,stressfulwork conditions, gender discrimination, social exclusion, unhealthy lifestyle, physical ill-health and human rights violations.[7]

According to the World Health Organization (WHO), in armed conflict generally, an estimated 17% and 15% of the population will suffer from depression and post-traumatic stress disorder (PTSD), respectively. Several other major studies in post-conflict, low-income countries have reported even higher rates of mental health challenges among the population. Indeed, a 2010 study covering a region of Liberia revealed that some 45% of the population exhibited symptoms of PTSD nearly 20 years after the end of the conflict.

Importantly, some studies have also shown a link between trauma exposure and views regarding conflict resolution, with one study on northern Uganda finding that PTSD was correlated with support for violence as a means of conflict resolution.[8]

Ample research demonstrates the links between trauma exposure, including war-related trauma exposure, and the emergence of psychological distress. The 2015 Global Burden of Disease study found a

positive association between conflict and depression and anxiety disorders. While most of those exposed to emergencies suffer some form of psychological distress, accumulated evidence shows that 15-20% of crisis-affected populations develop mild-to moderate mental disorders such as depression, anxiety, and post-traumatic stress.And,3-4%developseverementaldisorders,suchaspsychosisordebilitatingdepression and anxiety, which affect their ability to function and survive.[9]

AstudyofSudaneserefugeesinnorthernUgandafoundcorrelationsbetweenexposure to conflict, the prevalence of PTSD, and depressive and behavioral problems. It further found thattheday-to-dayhasslesoflifethechildrenexperiencedwerehigher,relativetochildren in theseameareawhohadnotexperiencedconflict.PTSDisalsoassociatedwithcomorbidity of wide-ranging symptoms, from attempted suicide, to bronchial asthma, hypertension, peptic ulcer, among others.[10]

AccordingtoInternationalOrganizationforMigration(10M),Overthelasttenyears, the Libyan people have suffered tremendously from conflict, indiscriminate violence, but also from direct attacks on health care facilities, schools, water resources, and residential areas.Damage and destruction of essential facilities consequently led to collapse of functionality of society and to a major economic crisis.[11]

Anotherresultfromthestudyrevealsthattheacademicperformanceofthe students are thesameforLevels1and3which have a verbal interpretation of "GOOD", andonlythe 2nd yearlevelgottheverbalinterpretationof "FAIR". Amidstcrisisanduncertainties,none from thedifferentyearlevelswereabletogetaverbalinterpretationof weak.Thoughthisresult is

agoodindicatorthatstudentscancopewiththeirstudies,wecannotdiscountthefact that we stillneedtopayattentiontodevelopingorenhancingtheircopingstrategiesandens uring for them to achieve their optimum mental health so as they can achieve their maximum potentials too in their academic performance.

Adolescents showing strong mental health have good social skills with both adults and peers, and their enhanced social and emotional behaviors have a strong impact on academic achievement. Therefore, mental health problems in adolescents may have an important influence on academic achievement, which in turn have lifelong consequences for employment, income, and other outcomes.

Frequent feelings of mental health problems exhibit school difficulties, including poor academic achievement. Adolescents displaying strong mental health are likely to have better academic achievement, compared to adolescents displaying weak mental health. [12]

The study showed a weak positive correlation between 2 variables, the mental health of the students and their academic performance.

Student life can be stressful and for some students it may cause mental distress. Besides being a major public health challenge, mental distress can influence academic achievement.[13]

Mental health problems can affect many areas of students' lives, reducing their quality of life, academic achievement, physical health, and satisfaction with the college experience, and negatively impacting relationships with friends and family members. These issues can also have

long-term consequences for students, affecting their future employment, earning potential, and overall health.[14]

Mental health problems can affect a student's energy level, concentration, dependability, mental ability, and optimism, hindering performance. Research suggests that depression is associated with lower grade point averages, and that co-occurring depression and anxiety can increase this association. Depression has also been linked to dropping out of school. [15]

Thepresentmeta-analysisaimedtodeterminetherelationshipbetweenmentalhealth and academic achievement in adolescents. This research, as expected, confirmed that there is a positive relationship between mental health and academic achievement. The research also indicated that mental health of adolescents is very important for schooling, in that it has a potentialtoinfluenceacademicachievementpositivelyornegatively.Therefore,it is deemed crucial for adolescents to have a strong mental health to perform better academically in school, which in turn have lifelong consequences for employment, income, and other outcomes. [16]

Accordingtothefindingsofthisresearch,itcanbeconcluded thatthe higher the mental health of the students, the better their educational performance. [17]

Ourresultsshowedthatmentalhealthwasastrongerpredictorofacademic performance than other predictors and students whose mental health improved made better academic progress than students whose mental health did not improve or worsened. [18]

CONCLUSIONS:

It can be said that the mental health of the students at the Faculty of Dentistry, Attahadi University was not that affected by the National Crisis on Libya. The results were not that high to affect their mental health status but it is still worthwhile to note that effects do exist and that mental health could be one area of concern to look into as WHO advocates a complete state of health.

It can be drawn that although the academic performance of some of the students are not that high, there was no weak or very weak in the results which proves that students are coping despite the crisis that they are experiencing.

Lastly, it can be said that the variables of the study correlates with each other, though it is just a weak relationship between variables, there is still a relationship that was established in the study and that we can still conclude that indeed the state of mental health of the student affects their academic performance.

REFERENCES:

1 - https://www.Aljazeera.com

2 - https://www.intechopen.com/

3 - https://www.euro.who.int/

4 - https://www.heretohelp.bc.ca/

5 - https://www.who.int/news-room/fact-sheets

6- https://www.medicalnewstoday.com/

7 - https://www.who.int/news-room/fact-sheets/

8 - 10- https://www.sanaacenter.org/

11 - https://www.Reliefweb.int

12 - https://www.intechopen.com/

13 - https://www.researchgate.net/publication

14 - https://www.sprc.org/

15 - https://www.sprc.org/colleges-universities/consequences

16 - https://www.intechopen.com/

17 - https://www.researchgate.net/publication

18 - https://www.ncbi.nlm.nih.gov/pmc/